ARTICLE

Dual Molecular Effects of Dominant *RORA* Mutations Cause Two Variants of Syndromic Intellectual Disability with Either Autism or Cerebellar Ataxia

Claire Guissart,[1,37] Xenia Latypova,[2,3,4,37] Paul Rollier,[5,37] Tahir N. Khan,[3,37] Hannah Stamberger,[6,7,8] Kirsty McWalter,[9] Megan T. Cho,[9] Susanne Kjaergaard,[10] Sarah Weckhuysen,[6,7,8] Gaetan Lesca,[11,12] Thomas Besnard,[2,4] Katrin Õunap,[13] Lynn Schema,[14] Andreas G. Chiocchetti,[15] Marie McDonald,[16] Julitta de Bellescize,[17] Marie Vincent,[2,4] Hilde Van Esch,[18] Shannon Sattler,[19] Irman Forghani,[20] Isabelle Thiffault,[21,22,23] Christine M. Freitag,[15] Deborah Sara Barbouth,[20] Maxime Cadieux-Dion,[21] Rebecca Willaert,[9] Maria J. Guillen Sacoto,[9] Nicole P. Safina,[23,24,25] Christèle Dubourg,[26] Lauren Grote,[23,24,25] Wilfrid Carré,[26] Carol Saunders,[21,22,23] Sander Pajusalu,[13]

(Author list continued on next page)

RORα, the RAR-related orphan nuclear receptor alpha, is essential for cerebellar development. The spontaneous mutant mouse *staggerer*, with an ataxic gait caused by neurodegeneration of cerebellar Purkinje cells, was discovered two decades ago to result from homozygous intragenic *Rora* deletions. However, *RORA* mutations were hitherto undocumented in humans. Through a multi-centric collaboration, we identified three copy-number variant deletions (two *de novo* and one dominantly inherited in three generations), one *de novo* disrupting duplication, and nine *de novo* point mutations (three truncating, one canonical splice site, and five missense mutations) involving *RORA* in 16 individuals from 13 families with variable neurodevelopmental delay and intellectual disability (ID)-associated autistic features, cerebellar ataxia, and epilepsy. Consistent with the human and mouse data, disruption of the *D. rerio* ortholog, *roraa*, causes significant reduction in the size of the developing cerebellum. Systematic *in vivo* complementation studies showed that, whereas wild-type human *RORA* mRNA could complement the cerebellar pathology, missense variants had two distinct pathogenic mechanisms of either haploinsufficiency or a dominant toxic effect according to their localization in the ligand-binding or DNA-binding domains, respectively. This dichotomous direction of effect is likely relevant to the phenotype in humans: individuals with loss-of-function variants leading to haploinsufficiency show ID with autistic features, while individuals with *de novo* dominant toxic variants present with ID, ataxia, and cerebellar atrophy. Our combined genetic and functional data highlight the complex mutational landscape at the human *RORA* locus and suggest that dual mutational effects likely determine phenotypic outcome.

Introduction

Nuclear receptors appeared in the metazoan lineage as an adaptation to multicellular organization requiring distant cellular signaling through non-peptidic growth and differentiation factors.[1] The nuclear receptor superfamily is a group of transcription factors regulated by small hydrophobic hormones, such as retinoic acid, thyroid hormone, and steroids.[2] Mutations in nuclear receptors cause a diverse range of disorders, including central nervous system (CNS) pathologies, cancer, and metabolic disorders. For example, haploinsufficiency of *RORB* (MIM: 601972), encoding the nuclear receptor RORβ, results in behavioral and cognitive impairment and epilepsy,[3] while biallelic mutations in *RORC* (MIM: 602943), encoding RORγ, result in immunodeficiency (MIM: 616622[4]). Nuclear Receptor Subfamily 0, Group B, Member 1 (NR0B1 [MIM: 300473]) is an orphan member of the nuclear receptor superfamily and has been implicated in sex reversal (MIM: 300018[5]) and congenital adrenal hypoplasia (MIM: 300200[6]). RORα (RORA) is most closely related to Retinoic Acid Receptor (RAR) yet functions differently; RAR acts as a ligand responsive heterodimer with retinoid X receptor (RXR). However, RORα isoforms 1 and 2 constitutively activate transcription and bind DNA as monomers at responsive elements which consist of 6-bp

[1]EA7402 Institut Universitaire de Recherche Clinique, and Laboratoire de Génétique Moléculaire, CHU and Université de Montpellier, 34093 Montpellier, France; [2]Service de Génétique Médicale, CHU Nantes, 9 quai Moncousu, 44093 Nantes Cedex 1, France; [3]Center for Human Disease Modeling, Duke University Medical Center, Durham, NC 27701, USA; [4]l'institut du thorax, INSERM, CNRS, UNIV Nantes, 44007 Nantes, France; [5]Service de Génétique Clinique, Centre Référence "Déficiences Intellectuelles de causes rares" (CRDI), Centre de référence anomalies du développement CLAD-Ouest, CHU Rennes, 35203 Rennes, France; [6]Division of Neurology, University Hospital Antwerp (UZA), 2610 Antwerp, Belgium; [7]Neurogenetics Group, Center for Molecular Neurology, VIB, 2650 Antwerp, Belgium; [8]Laboratory of Neurogenetics, Institute Born-Bunge, University of Antwerp, 2650 Antwerp, Belgium; [9]GeneDx, 207 Perry Parkway, Gaithersburg, MD 20877, USA; [10]Chromosome Laboratory, Department of Clinical Genetics, Copenhagen University Hospital, Rigshospitalet, 2100 Copenhagen, Denmark; [11]Service de génétique, Groupement Hospitalier Est, Hospices Civils de Lyon, Lyon, France; [12]INSERM U1028, CNRS UMR5292, Centre de Recherche en Neurosciences de Lyon, Université Claude Bernard Lyon 1, Lyon, France; [13]Department of Clinical Genetics, United Laboratories, Tartu University Hospital and Institute of Clinical Medicine, University of Tartu, 2 L.Puusepa street, Tartu 51014, Estonia; [14]University of Minnesota-Fairview, Minneapolis, MN 55454, USA; [15]Department of Child and Adolescent Psychiatry, Psychosomatics and Psychotherapy, JW Goethe

(Affiliations continued on next page)

Emily Farrow,[21,23,24] Anne Boland,[27] Danielle Hays Karlowicz,[16] Jean-François Deleuze,[27] Monica H. Wojcik,[28] Rena Pressman,[20] Bertrand Isidor,[2,4] Annick Vogels,[18] Wim Van Paesschen,[29] Lihadh Al-Gazali,[30] Aisha Mohamed Al Shamsi,[31] Mireille Claustres,[1] Aurora Pujol,[32] Stephan J. Sanders,[33] François Rivier,[34] Nicolas Leboucq,[35] Benjamin Cogné,[2,4] Souphatta Sasorith,[1] Damien Sanlaville,[11,12] Kyle Retterer,[9] Sylvie Odent,[5,36] Nicholas Katsanis,[3] Stéphane Bézieau,[2,4] Michel Koenig,[1,38] Erica E. Davis,[3,38,*] Laurent Pasquier,[5,38] and Sébastien Küry[2,4,38,*]

AT-rich sequences.[7] The amino-terminal domain of the RORα1 isoform determines its affinity and specific DNA-binding properties by acting in concert with the zinc finger domain.[7]

RORα deficiency is known to cause the mouse *staggerer* (*sg*) phenotype, a cerebellar degenerative model.[8] In humans, microdeletions overlapping *RORA* on 15q22.2 have been reported in affected individuals as part of a contiguous gene syndrome,[9] with the smallest deletion involving two genes, NMDA receptor-regulated 2 (*NARG2/ICE2*) and *RORA*. All reported individuals with 15q22.2 microdeletion share epileptic seizures, mild intellectual disability (ID), and dysmorphic features, with variable ataxia.[9] Here, we report 16 affected individuals from 13 syndromic ID-affected families with intergenic or intragenic deletions, truncating mutations, or missense changes in *RORA*. We modeled these genetic findings in zebrafish larvae through endogenous *roraa* ablation or heterologous expression of *RORA*, followed by relevant cerebellar phenotyping. In zebrafish models, we recapitulated the neuroanatomical features of affected humans as well as the *staggerer* mouse, and we show that loss of *roraa* leads to reduction of both the Purkinje and granule compartments of the cerebellum. Further, our *in vivo* data indicate that missense variants in the DNA binding domain confer a dominant toxic effect, while a missense change in the ligand binding domain results in a loss-of-function effect. Together, our data highlight how different mutation effects at the *RORA* locus can produce overlapping but distinct phenotypic outcomes.

Subjects and Methods

Genetic Studies and Ethics Statement

Human genetic studies conducted in research laboratories were approved by local ethics committees from participating centers (Antwerp, Belgium; Lyon, France; Frankfurt, Germany; Copenhagen, Denmark; Montpellier, France; Tartu, Estonia; Minneapolis and Kansas City, USA). Written informed consent was obtained from all study participants. All 16 affected individuals underwent extensive clinical examination by at least one expert clinical geneticist. Routine genetic testing was performed whenever clinically relevant, including copy-number variation (CNV) analysis by high-resolution array-based comparative genomic hybridization (aCGH) using (1) 180k CytoSure ISCA v2 array (Oxford Gene Technology; individuals 10A–D), (2) 180k SurePrint G3 CGH microarray as described[10] (Agilent; individual 11), or (3) 400k SurePrint G3 CGH microarray, as described[11] (Agilent, individuals 12 and 13). Affected individuals with a negative aCGH result underwent whole-exome sequencing (WES) on an Illumina HiSeq platform according to the following paradigms: (1) trio-based clinical diagnostic WES (individuals 1, 2, 6, 7, and 9), (2) trio-based WES in a research laboratory (individuals 3 and 4), or (3) WES of an affected individual followed by single site testing in parental DNA samples (individuals 5 and 8; see Table S1 for further details). Point mutations were confirmed by Sanger sequencing of DNA sample from all available family members, when possible.

Establishment and Culture of Primary Fibroblasts

We conducted biochemical studies in primary cultures of skin fibroblasts from individuals 2, 3, and 6 and from two control individuals (WT1 and WT2). Fibroblasts were grown in RPMI 1640 medium, containing 5% fetal calf serum (FCS, ThermoFisher, Waltham), 2 mM L-glutamine (ThermoFisher), 1% Ultroser G

University Frankfurt, Deutschordenstraße 50, Frankfurt am Main 60528, Germany; [16]Division of Medical Genetics, Department of Pediatrics, Duke University, Durham, NC 27710, USA; [17]Epilepsy, Sleep and Pediatric Neurophysiology Department, Hospices Civils, Lyon, 69677 Bron, France; [18]Center for Human Genetics, University Hospitals Leuven, Herestraat 49, 3000 Leuven, Belgium; [19]Carle Physician Group, Urbana, IL 61801, USA; [20]Dr. John T. Macdonald Foundation Department of Human Genetics, University of Miami, Miller School of Medicine, 1501 NW 10th Avenue, BRB, room 359 (M-860), Miami, FL 33136, USA; [21]Center for Pediatric Genomic Medicine, Children's Mercy Hospital, Kansas City, MO 64108, USA; [22]Department of Pathology and Laboratory Medicine, Children's Mercy Hospital, Kansas City, MO 64108, USA; [23]University of Missouri Kansas City, School of Medicine, Kansas City, MO 64108, USA; [24]Division of Clinical Genetics, Children's Mercy Hospital, Kansas City, MO 64108, USA; [25]Department of Pediatrics, Children's Mercy Hospital, Kansas City, MO 64108, USA; [26]Laboratoire de Génétique Moléculaire & Génomique, CHU de Rennes, 35033 Rennes, France; [27]Centre National de Recherche en Génomique Humaine (CNRGH), Institut de Biologie François Jacob, DRF, CEA, Evry, France; [28]The Broad Institute of MIT and Harvard, Cambridge, MA 02142, USA; [29]Department of Neurology, University Hospitals Leuven, Herestraat 49, 3000 Leuven, Belgium; [30]Department of Paediatrics, College of Medicine and Health Sciences, United Arab Emirates University, PO Box 17666, Al Ain, United Arab Emirates; [31]Department of Paediatrics, Tawam Hospital, PO Box 15258, Al-Ain, United Arab Emirates; [32]Neurometabolic Diseases Laboratory, IDIBELL, Gran Via, 199, L'Hospitalet de Llobregat, 08908 Barcelona, and CIBERER U759, Center for Biomedical Research on Rare Diseases, 08908 Barcelona, Spain, Catalan Institution of Research and Advanced Studies (ICREA), 08010 Barcelona, Spain; [33]Department of Psychiatry, UCSF Weill Institute for Neurosciences, University of California, San Francisco, San Francisco, CA 94158, USA; [34]Department of Neuropaediatrics and CR Maladies Neuromusculaires, CHU Montpellier, PhyMedExp, INSERM, CNRS, University of Montpellier, Montpellier, France; [35]Neuroradiologie, CHU de Montpellier, 34090 Montpellier, France; [36]CNRS UMR 6290, Université de Rennes, 2 Avenue du Professeur Léon Bernard, 35043 Rennes, France
[37]These authors contributed equally to this work
[38]These authors contributed equally to this work
*Correspondence: erica.davis@duke.edu (E.E.D.), sebastien.kury@chu-nantes.fr (S.K.)
https://doi.org/10.1016/j.ajhg.2018.02.021.

(Pall, Cortland), 1 × Antibiotic-Antimycotic (ThermoFisher) and were maintained in a humidified incubator at 37°C/5% CO_2. Both RT-PCR and western blotting studies were performed using individual fibroblasts plated in 6-well plates (200,000 cells/well).

RT-PCR Studies in Primary Fibroblasts

Total RNA was extracted using the RNeasy Plus Mini kit (QIAGEN) and reverse transcribed with the Moloney Murine Leukemia Virus Reverse Transcriptase (ThermoFisher). PCR amplification was performed with primers located in exons 3 and 4 (Table S2) and the Promega MasterMix (Promega). PCR products were separated on a 1.5% agarose gel and fragments were cut from the gel. After extraction from gel slices, the PCR products were purified with ExoSAP-IT (ThermoFisher) and sequenced by standard cycle-sequencing reactions with Big Dye terminators (ThermoFisher) with the PCR forward and reverse primers in an ABI PRISM 3130xl Genetic Analyzer (Applied Biosystems). Mutation detection analysis was performed using 4Peaks.

RORA Immunoblotting

Total protein lysate was extracted from primary fibroblasts using 1 × Laemmli buffer. Proteins were separated on 10% SDS-PAGE gels and transferred to PVDF membrane (Westran Clear Signal Whatman; Dominique Dutscher, Brumath). The membranes were incubated overnight with 1:200 diluted anti-RORα (sc-6062, Santa Cruz biotechnology) primary antibody in 5% skim milk. Protein levels of the housekeeping protein GAPDH were assayed for internal control of protein loading with 1:1,000 diluted GAPDH antibody (sc-25778, Santa Cruz Biotechnology).

Three-Dimensional (3D) Protein Modeling

Missense changes located in the DNA-binding domain of RORA isoform a were studied by 3D modeling. Wild-type (WT) and mutated RORA DNA binding domain homology models were generated according to the crystal structure of the RXR-RAR DNA-binding complex on the retinoic acid response element DR1 using Modeler[12] software with standard parameters.

RORA Expression Analysis in Neuronal Cell Types

There are four RefSeq transcripts of *RORA* (GenBank): NM_134261.2 (*RORA* 1), NM_134260.2 (*RORA* 2), NM_002943.3 (*RORA* 3), and NM_134262.2 (*RORA* 4). Relative mRNA levels of the four *RORA* transcripts were assessed in three different commercially obtained human cDNAs by quantitative (q)RT-PCR: (1) cerebellar cDNA from a 26-year-old male (Amsbio), (2) whole-brain cDNA pooled from two males of Northern European descent aged 43–55 years, Human multiple tissue cDNA (MTC) panel I (Clontech), and (3) Human Universal QUICK-Clone II (Clontech) using transcript-specific primers (Table S2) and SYBR Green PCR Master Mix (Thermo Fisher) on an ABI 7900HT real-time PCR system. We determined relative gene expression levels in quadruplicate samples according to the ΔCt method. After normalization to *β-actin* levels, $-\log^2$ of ΔCt for each of the four transcripts was added together to determine total expression levels from the *RORA* locus for each cDNA. Relative *RORA* transcript expression levels expressed in $-\log^2$ of ΔCt were obtained by calculating the percentage of each transcript compared to total *RORA* expression.

Zebrafish Lines and Husbandry

All zebrafish work was performed in accordance with protocols approved by the Duke University Institutional Animal Care and Use Committee. Zebrafish embryos were obtained by natural matings of WT (ZDR strain, Aquatica BioTech) or transgenic (*neurod:egfp*) adults[13] and maintained on a 14 hr/10 hr light-dark cycle. Embryos were reared in embryo media (0.3 g/L NaCl, 75 mg/L $CaSO_4$, 37.5 mg/L $NaHC0_3$, 0.003% methylene blue) at 28°C until processing for phenotypic analyses at 3 days post-fertilization (dpf).

CRISPR/Cas9 Genome Editing of *roraa* in Zebrafish

We designed two guide (g) RNAs targeting *roraa* (GRCz10: ENSDARG00000031768) using the CHOPCHOP v2 tool[14] and synthesized them *in vitro* with the GeneArt precision gRNA synthesis kit (Table S2; Thermo Fisher) as described.[15–17] We targeted the *roraa* locus by microinjection into the cell of zebrafish embryos with 1 nL of cocktail containing 100 pg gRNA and 200 pg Cas9 protein (PNA Bio) at the 1-cell stage. We harvested individual embryos (n = 8) at 1 dpf for DNA extraction to assess targeting efficiency. We PCR-amplified the region flanking the targeted site (Table S2), denatured the resulting product, and reannealed it slowly to form heteroduplexes (95°C for 5 min, ramped down to 85°C at 1°C/s and then to 25°C at 0.1°C/s). We performed polyacrylamide gel electrophoresis (PAGE) on a 20% precast 1 mm gel (Thermo Fisher) to visualize heteroduplexes. To estimate mosaicism of F0 mutants, PCR products were cloned into a TOPO-TA vector (Thermo Fisher) and individual colonies (n = 24) were sequenced (n = 3 larvae/gRNA).

Transient *roraa* Suppression, *In Vivo* Complementation, and Heterologous Expression Experiments

We designed splice blocking (sb) morpholinos (MO) targeting either the splice donor site of exon 2 (e2i2) or exon 3 (e3i3) of *roraa* (GeneTools, LLC; Table S2) and injected 1 nL of MO into the yolk of zebrafish embryos at 1- to 4-cell stage. To confirm expression of the two annotated *roraa* transcripts (GRCz10: ENSDART00000148537.2 and ENSDART00000121449.2) and to determine MO efficiency, we harvested uninjected control and MO-injected larvae in Trizol (Thermo Fisher) at 3 dpf, extracted total RNA, and conducted first-strand cDNA synthesis with the QuantiTect Reverse Transcription kit (QIAGEN). The targeted region of *roraa* was PCR amplified using primers complementary to sites in flanking exons (Table S2) and migrated by electrophoresis on a 1% agarose gel; bands were excised, gel purified using QIAquick gel extraction kit (QIAGEN) and resulting clones were Sanger sequenced. The optimal MO dose for *in vivo* complementation experiments was determined by injection of three concentrations of MO (2, 3, 4 ng of e2i2; or 6, 7, 8 ng of e3i3). To generate mRNA for injections, we purchased Gateway-compatible open reading frame (ORF) clones from Genecopoeia (*RORA* 1, *RORA* 2, and *RORA* 3) or Thermo Fisher (*RORA* 4) and transferred the ORFs to a pCS2+ vector by LR clonase II-mediated recombination (Thermo Fisher). We performed site-directed mutagenesis of *RORA* 4 according to the QuikChange protocol (Table S2; Agilent), using described methodology;[18] sequences were validated by Sanger sequencing. Linearized pCS2+ vectors containing WT or mutant ORFs were transcribed *in vitro* with the mMessage mMachine SP6 Transcription kit (Ambion).

Whole-Mount Immunostaining

We stained axonal tracts of the cerebellum with monoclonal anti-acetylated tubulin antibody produced in mouse (Sigma-Aldrich, T7451, 1:1,000), as described.[19] We fixed larvae in Dent's solution (80% methanol and 20% DMSO) and carried out primary antibody detection overnight and secondary detection for 1 hr with

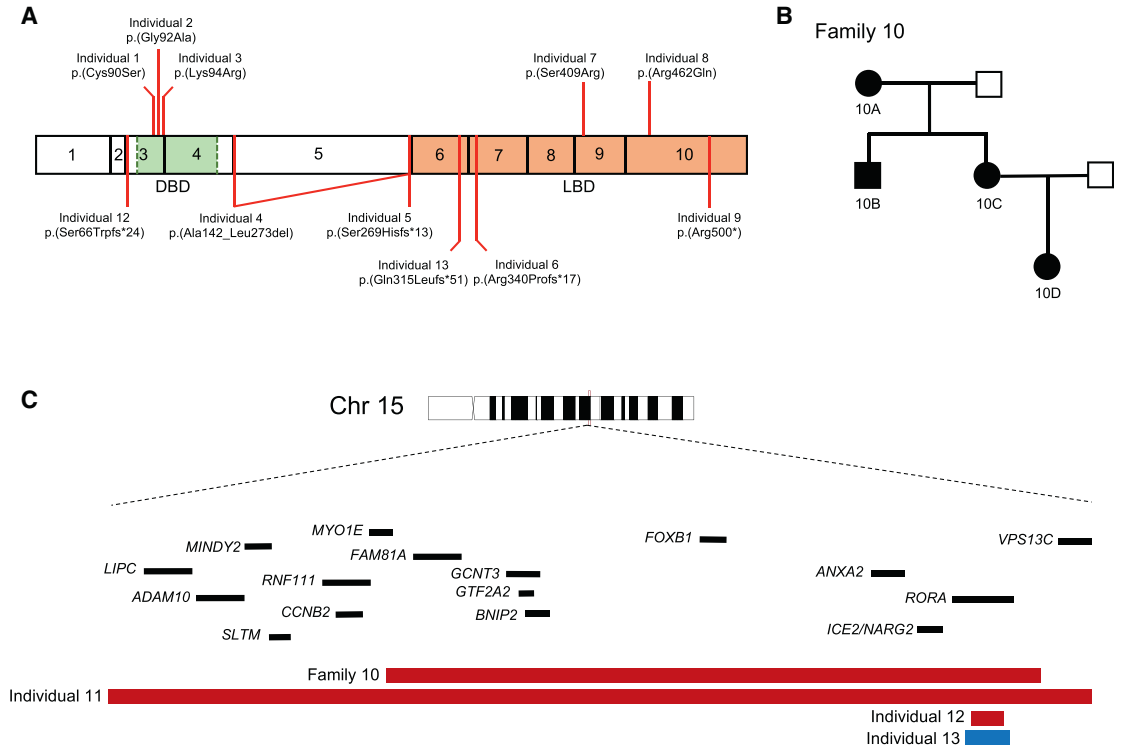

Figure 1. *RORA* Variants Cause Intellectual Disability with Autistic Features or Cerebellar Hypoplasia
(A) Schematic of RORα isoform a (GenBank: NP_599023.1; encoded by *RORA* transcript 1) depicting exons (black outlined boxes with numbers 1–10) and domains; green, DNA binding domain (DBD); orange, ligand binding domain (LBD). Missense variants (top) and truncating variants (bottom) are shown.
(B) Autosomal-dominant pedigree (family 10) in which a ~1.5 Mb intergenic deletion containing *RORA* segregates with disease. Filled shapes, affected individuals; unfilled shapes, healthy individuals. Individuals 10A, 10B, 10C, 10D, and the spouse of 10C were tested.
(C) Schematic depicting the *RORA* locus at 15q22. Zoomed region shows two intergenic deletions (individuals 10A–D and individual 11), one intragenic deletion (individual 12), and an intragenic duplication (individual 13) involving *RORA*. Genes are indicated by black bars; copy number loss, red; copy number gain, blue.

Alexa Fluor 488 goat anti-mouse IgG (A11001, Invitrogen; 1:1,000). We visualized the Purkinje compartment of the zebrafish cerebellum with anti-zebrin II antibody (a gift from Dr. Richard Hawkes) in *neurod:egfp* transgenic larvae. Briefly, zebrafish larvae were fixed in 4% paraformaldehyde and incubated overnight in mouse anti-zebrin II antibody (1:100); secondary antibody was applied for 1 hr (Alexa Fluor 594 goat anti-mouse IgG, A11005, Invitrogen; 1:1,000). Fluorescent signal was imaged manually on dorsally positioned larvae using an AxioZoom.V16 microscope and Axiocam 503 monochromatic camera, using Zen Pro 2012 software (Zeiss). Cerebellar structures of interest or optic tecta were measured using ImageJ.[20] Total cerebellar area was measured on acetylated tubulin-stained larvae by outlining structures with fluorescent signal; regions comprised of Purkinje cells were measured on zebrin II-stained regions; region comprised of granule cells were measured on GFP-positive regions. Statistical analyses were performed using a two-tailed parametric t test (GraphPad software).

Results

Identification of Point Mutations or Copy-Number Variants Disrupting RORA

As part of our ongoing studies to understand the molecular basis of neurodevelopmental disorders, we identified a total of 16 individuals with rare variants suspected to alter *RORA* function (Figure 1; Tables 1, S3, and S4). The first individual under investigation was a female with severe syndromic ID, multifocal seizures, mild cerebellar hypoplasia, and hypotonia (individual 6, Table 1; Figure 2A). Upon performing WES, we identified a *de novo* frameshifting mutation in *RORA* (GenBank: NM_134261.2; c.1019delG [p.Arg340Profs*17]) that was not present in the genome aggregation database (gnomAD; >246,000 chromosomes) or the NHLBI Exome Variant Server (EVS; >13,000 alleles). Information exchange on community data-sharing platforms including GeneMatcher,[21] the DatabasE of genomiC varIation and Phenotype in Humans using Ensembl Resources (DECIPHER), and the Broad Institute matchbox repository facilitated the identification of an additional 15 affected individuals with *RORA* variants who displayed overlapping phenotypes. These variants were present *de novo* in 11 simplex families with affected individuals and segregated in one three-generation pedigree under a dominant paradigm, bolstering the candidacy of this locus. Of note, segregation analysis was impossible in individual 1's family, since the child had been adopted.

Of the 16 affected individuals, 4 harbored likely pathogenic SNVs predicted to alter RORA protein sequence or

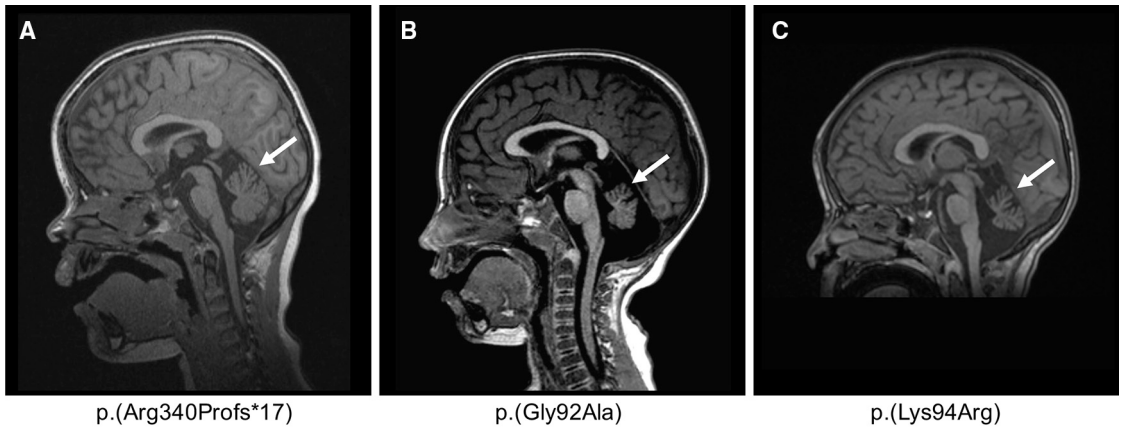

Figure 2. Brain MRI of Individuals with Cerebellar Hypoplasia
MRI of individual 6 done at 6.5 years old (A), individual 2 done at 2 years and 1 month old (B), and individual 3 done at 2 years old (C) showing cerebellar hypoplasia, predominant on the vermis (white arrow). T1-weighted sequence, sagittal section through cerebellum.

dose. In addition to individual 6, three affected individuals had *de novo* SNVs or small indels in *RORA*; these included one frameshifting mutation, one nonsense mutation, and one mosaic canonical splice acceptor site change (Figure 1A; Tables 1 and S3). These three *RORA* variants are predicted to result in protein sequence with either complete (c.804_805delGT [p.Ser269Hisfs*13]) or partial (c.1019delG [p.Arg340Profs*17] and c.1498C>T [p.Arg500*]) truncation of the ligand binding domain at the C terminus and/or nonsense-mediated mRNA decay (NMD). Notably, analyses of fibroblast protein lysates from individual 6 (p.Arg340Profs*17) showed that RORA protein levels were not decreased compared to control subjects, suggesting that related mRNA harboring the premature stop codon would not be eliminated by NMD. According to Alamut software (compiling five different prediction tools: Splicesite Finder-like, MaxEntScan, NNSPLICE, GeneSplicer, and Human Splicing Finder), the splice acceptor site mutation, c.425−1G>A, is predicted to cause in-frame exon skipping and deletion of 77 amino acids (p.Ala142_Leu273del); however, cell lines were unavailable from the affected individual to confirm this prediction; mosaicism was estimated at about 20% from exome and Sanger sequencing data.

An additional seven affected individuals had non-recurrent CNVs impacting the *RORA* locus detected by high-resolution aCGH (Tables 1 and S4; Figures 1A–1C and S1). We identified one ~63 kb duplication interrupting *RORA* exons 3–6, which is predicted to result in a premature termination of the protein (p.Gln315Leufs*51), one intragenic CNV that resulted in a ~27 kb deletion of *RORA* exon 3 and its flanking intronic regions to produce a putative frameshifting truncation, and one ~3.7 Mb intergenic deletion impacting 17 genes on 15q22.3q22.2 including *RORA*. Segregation in each of the three families showed that all three CNVs occurred *de novo*. Furthermore, we detected a ~1.5 Mb intergenic deletion in four individuals segregating neurological phenotypes in an autosomal-dominant pedigree (Figure 1B); this CNV encompasses nine genes, including *RORA*.

Finally, an additional five affected individuals had missense mutations predicted to be deleterious (Tables 1 and S3; Figure S2). All five alleles were absent from all available public databases queried (gnomAD, ExAC, EVS). Two of the five variants, c.1225A>C (p.Ser409Arg) and c.1385G>A (p.Arg462Gln), map to the ligand binding domain; both residues are conserved in vertebrate orthologs of RORα but not in the human paralogous nuclear receptor proteins, indicating that these positions are specific to the ROR sub-family. The other three variants—c.269C>G (p.Cys90Ser), c.275G>C (p.Gly92Ala), and c.281A>G (p.Lys94Arg)—are located in the conserved zinc-finger DNA-binding domain of RORα. The three residues Cys90, Gly92, and Lys94, together with Cys93, belong to the P box motif that is part of the alpha-helix of the first zinc-finger domain of the nuclear receptors and interacts directly with DNA (Figure S3A).[22] Because the c.281A>G variant lies in the donor splice site of exon 3, we examined whether it impacts mRNA splicing in primary skin fibroblasts from individual 3; RT-PCR showed neither abnormal sized product nor semiquantitative differences in cDNA amounts (Figures S4A and S4B). Additionally, western blotting of lysates from primary fibroblasts harboring the c.275G>C change (individual 2) showed a modest increase of RORα levels when compared to a matched control (Figure S4C).

Clinical Features of Individuals with RORA Variants

The 16 affected individuals in our cohort display complex phenotypes with regards to their cognition, motor function, and electrophysiology (Table 1). The predominant phenotype was ID. However, cognitive function was variable among the 16 individuals and ranged from mild to moderate (13/16) to severe (2/16), while one individual had a low intelligence quotient (IQ) without ID. We noted IQ regression in one affected individual (individual 4) who had cognitive decline at ~10 years

Table 1. Molecular and Clinical Data from the 15 Individuals with *RORA* Variants

Individual ID	1	2	3	4	5	6	7
DECIPHER ID	–	–	–	–	–	–	–
Sex	female	male	female	female	female	female	male
Geographic origin	USA	Estonia	France	USA	USA	France	USA
Age at last investigation (years)	4	3.5	6	28	3	10	9
Mutation type	missense	missense	missense	splice site	frameshift	frameshift	missense
Mutation (GRCh37)[a]	c.269G>C	c.275G>C	c.281A>G	c.425-1G>A	c.804_805delGT	c.1019delG	c.1225A>C
Protein variant[b]	p.Cys90Ser	p.Gly92Ala	p.Lys94Arg	p.Ala142_Leu273del	p.Ser269Hisfs*13	p.Arg340Profs*17	p.Ser409Arg
Mode of inheritance	unknown (adopted)	*de novo*	*de novo*	*de novo* (mosaic, 20% in blood) [c]	*de novo*	*de novo*	*de novo*
Functional effect[d]	NA	dominant toxic	dominant toxic	NA	NA	NA	NA
Growth Parameters							
Birth weight (grams/SD)	NA	3,500/0	3,310/0	4,238/+2	4,054/+1.4	2,655/−1.5	3,487/0
Birth length (cm/SD)	NA	52/+1	49/0	NA	54.6/+1.9	46/−2	52/+1
Birth head circumference (cm/SD)	NA	38/+2.5	34.5/0	NA	NA	33/−1	34/−0.5
Height at age last investigation (cm/SD)	102/0	102/+0.5	104/−2	167.8/+0.5	89/−1.5	132/−1	120.8/−2 (8 y 5 mo)
Weight at age last investigation (kg/SD)	17.2/+0.5	17.8/+1	16/−1.5	69.4/+1	14.5/+0.3	26.2/−1.3	31/+1.3 (9 y 3 mo)
Head circumference at age last investigation (cm/SD)	49/0	50.6/0	50/0	58.4/+1.9	NA	53/0	51.7/−0.3 (8 y 4 mo)
Degree of developmental delay or ID	mild	mild-moderate	severe	mild (regression at 10 years)	mild	severe	mild
Age of walking	2 years	3 years	6 years	14 months	20 months	3 years	15 months
Age of first words	2 years	delayed	before 1 year	14–15 months	12–13 months	5 years	>2 years
Current language ability	speaking with sentences	speaking with sentences	no phrase	normal	around 20 words	no phrase	delayed
Behavioral anomalies	no	no	no	no	ASD	ASD	ASD

(*Continued on next page*)

8	9	10D	10C	10B	10A	11	12	13
–	–	–	–	–	**289628**	–	**255754**	**293939**
male	male	female	female	male	female	male	male	male
Germany	USA	Belgium	Belgium	Belgium	Belgium	France	Denmark	Denmark
4	14	25	50	44	80	15	8	6,5
missense	nonsense	15q22 deletion including *RORA*	15q22 deletion including *RORA*	15q22 deletion including *RORA*	15q22 deletion including *RORA*	15q22.3q22.2 deletion including *RORA*	15q22 intragenic deletion of *RORA*	15q22 disruptive duplication of *RORA*
c.1385G>A	c.1498C>T	15q22.2 (59,641, 986-61,104, 231) x1	15q22.2 (59,641, 986-61, 104,231) x1	15q22.2 (59,641, 986-61, 104,231) x1	15q22.2 (59,641, 986-61, 104,231) x1	15q21.3q22.2 (58,622,268 −62,320,616) x1	15q22.2 (60,809, 984-60,837, 029) x1	15q22.2 (60,797, 691-60,860, 668) x3
p.Arg462Gln	p.Arg500*	–	–	–	–	–	p.Ser66Trpfs*24	p.Gln315Leufs*51
de novo	*de novo*	dominant; inherited from mother (ID 10C)	dominant; inherited from mother (ID 10A)	dominant; inherited from mother (ID 10A)	dominant	*de novo*	*de novo*	*de novo*
loss-of-function	NA	NA	NA	NA	NA	NA	NA	NA
NA	3,340/−0.4	NC/+0.7	NA	NA	NA	3,200/−0.5	4050/+1	NC; unremarkable
NA	48.3/−0.7	NC/+0.7	NA	NA	NA	49.5/0	56/+2.5	NC; unremarkable
NA	46.5/+2 (6 mo)	NC/+0.7	NA	NA	NA	34/−0.5	NA	NC; unremarkable
NA	150.4/−0.7 (13 y)	166/+0.7	NA	NA	NA	170/0	NC/+2.5	NC/−1
NA	44.4/−0.2 (13 y)	74.3/+1.3	NA	NA	NA	58/+0.7	NC/+1	NC/−1
NA	58/+2.6 (13 y)	54/−0.7	NA	NA	NA	56/+0.7	NA	NA
no ID (IQ 85)	moderate	mild	mild	mild	mild	moderate	mild	mild
NA	24 months	16 months	NA	NA	NA	21 months	normal	mild delay
NA	delayed	14 months	NA	NA	NA	2 years	delayed	delayed
normal	rudimentary sentences	delayed	NA	NA	NA	normal	delayed	delayed
ASD	no	behavioral problems	no	borderline personality disorder	no	hyperactivity	no	ASD

(*Continued on next page*)

Table 1. ***Continued***

Individual ID	1	2	3	4	5	6	7
DECIPHER ID	–	–	–	–	–	–	–
Neurological Examination							
Seizures (age at onset/type)	no	no	yes (4 years/ absences)	yes (8 years/ tonic-clonic seizures)	yes (ND/ 1 episode of absence)	yes (5 years/ multifocal)	yes (neonatal/ myoclonic seizures)
Neurological examination	tremor, hypotonia, coordination disorder	tremor, hypotonia, ataxia	tremor, hypotonia, ataxia, pyramidal syndrome	tremor, hypotonia, ataxia	hypotonia, poor coordination	tremor, hypotonia, ataxia	occasional fine tremor
Brain imaging	normal	cerebellar hypoplasia (mainly vermis)	pontocerebellar atrophy (mainly vermis)	NA	normal	mild global cerebellar hypoplasia	corpus callosal hypoplasia
Global Examination							
Eye anomalies	strabismus, esotropia, nystagmus, amblyopia	no	mild oculomotor apraxia, strabismus	visual processing deficits	no	no	esotropia, hyperopia
Other	–	spina bifida occulta	recurrent vomiting, constipation	hypoglycemia in childhood	bilateral hydronephrosis	hypercholesterolemia	popliteal contractures
Other genetic findings	VUS in *NR4A2*	–	maternally inherited heterozygous p.(Arg662*) in *DNM1L*	–	maternally inherited deletions of 3p26.3 and 10q21.3 (both classified as VUS), mother reports no history of developmental delays	–	*HSPG2* c.7006+1G>A (maternally inherited), *HSPG2* c.4391G>A (paternally inherited), *GSK3B* c.625dupC (*de novo*), *CACNA1A* c.5883G>A (maternally inherited)
Initial diagnostic hypotheses	none	ID and disorders with cerebellar involvement	congenital ataxia with pontocerebellar atrophy	disorder of mitochondrial metabolism	none	none	speech delay, toe walking

Abbreviations: LoF, loss of function; GoF, gain of function; ND, not determined; ASD, autism spectrum disorder; ID, intellectual disability; IQ, intelligence quotient; GGE, genetic generalized epilepsy; NA, not analyzed; NC, not communicated; ND, not determined; y, years.
[a]Nomenclature HGVS V2.0 according to mRNA reference sequence GenBank: NM_134261.2. Nucleotide numbering uses +1 as the A of the ATG translation initiation codon in the reference sequence, with the initiation codon as codon 1.
[b]Inferred from bioinformatic predictions but not verified from the individual's mRNA.
[c]Mosaicism was inferred and estimated initially from raw exome sequencing data and confirmed by Sanger sequencing.
[d]Effect inferred from *in vivo* tests in zebrafish or analyses from patient fibroblasts; *in vitro* experiments.

of age. Developmental milestones were also delayed. The mean age of walking was delayed in 8/12 individuals; 11/12 walked by 3 years of age. Further, 11/13 individuals had speech delay and/or poor verbal communication abilities, and 2 were not speaking in sentences by the age of 6. We diagnosed epilepsy in 11/16 individuals (Table 1); the predominant seizure semiology was that of a generalized epilepsy with absences, drop attacks, and tonic-clonic seizure sub-types. None of the patients with *RORA* intragenic mutation had overt dysmorphic facial features. Of the nine individuals who underwent brain MRI, six had normal results and three were diagnosed with cerebellar hypoplasia, which predominantly affected the vermis (individuals 2 and 3; Figures 2B and 2C). These individuals developed early-onset ataxia and hypotonia by age 1.

Modeling RORA Disruption in Zebrafish

To corroborate the *Rora*^{sg} mouse mutant phenotype data[8,23] and to determine the effect of missense variants identified in affected individuals, we developed zebrafish models of *RORA* ablation and expression. We and others have shown previously that zebrafish is a robust model of neuroanatomical phenotypes observed in humans.[19,24–26] In particular,

8	9	10D	10C	10B	10A	11	12	13
–	–	–	–	–	**289628**	–	**255754**	**293939**
no	yes (ND/ generalized seizures)	yes (4 years/ absences, drop attacks)	yes	yes (ND/ generalized, *status epilepticus*)	no	yes (ND/ generalized, febrile seizures)	no	yes
NA	mild hand tremor, hypotonia	NA	NA	tremor	no	palpebral myoclonia	no	no
NA	CSF spaces mildly prominent	normal	NA	normal	NA	NA	NA	NA
NA	strabismus, hyperopia	strabismus	strabismus	NA	NA	strabismus	no	no
–	cryptorchidism, renal cysts	–	–	–	–	–	atopic dermatitis	–
–	*NGLY1* c.1516C>T, p.Arg506* (maternally inherited), *PKD2* c.2143delC, (p.Leu715*) (paternally inherited), 3p26.2 deletion (maternally inherited; VUS)	intragenic *DISC1* deletion (1q42.2(231, 834,554–231, 885,282)x1	intragenic *DISC1* deletion (1q42.2(231, 834,554–231, 885,282)x1	intragenic *DISC1* deletion (1q42.2(231, 834,554–231, 885,282)x1	intragenic *DISC1* deletion (1q42.2(231, 834,554–231, 885,282)x1	–	–	–
idiopathic ASD F84.0	*CUL4B*-related disorder	GGE and ID	ID and possible epilepsy	ID?	epilepsy (GGE?) and ID	deletion of *RORB*	none	none

assay of cerebellar defects in zebrafish has provided crucial insights toward understanding underlying pathomechanism,[27–29] especially given the high conservation of granule and Purkinje cell types between mammals and teleost species.[30] First, we aimed to model *RORA* disruption *in vivo* by targeting and knocking down the relevant zebrafish ortholog. Through reciprocal BLAST of the zebrafish genome and four annotated human *RORA* transcripts (GenBank: NM_134261, NM_134260, NM_002943, and NM_134262; Figure S5A), we identified two zebrafish orthologs: *roraa* (Ensembl ID: ENSDARG00000031768; GRCz10; 88%, 91%, 91%, and 91% identity to proteins encoded by *RORA* 1, *RORA* 2, *RORA* 3, *RORA* 4, respectively) and *rorab* (Ensembl ID: ENSDARG00000001910; 69%, 72%, 72%, and 73% identity to *RORA* 1, *RORA* 2, *RORA* 3, *RORA* 4, respectively). Next, we considered endogenous expression data to determine the most appropriate *D. rerio* transcript(s) to modulate *in vivo*. RNA *in situ* hybridization studies in zebrafish larvae have documented *roraa* expression patterns in the developing cerebellum as well as other anterior structures (optic tecta, hindbrain, and retina). However, *rorab* expression is restricted to the hindbrain.[31,32] Considering both the amino acid conservation and also the spatiotemporal expression of *roraa* in the

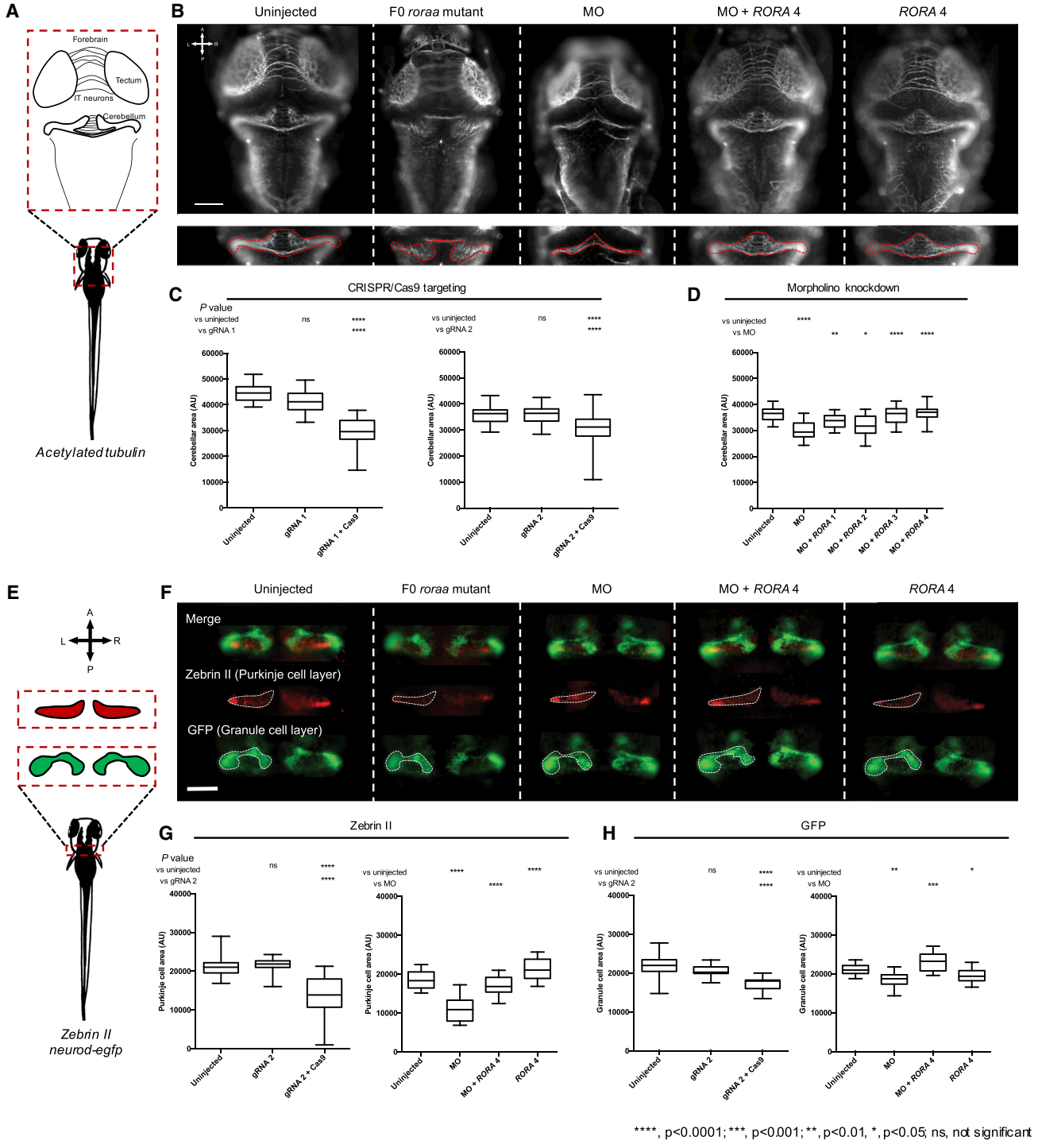

Figure 3. Disruption of *roraa* in Zebrafish Larvae Results in Cerebellar Hypoplasia Driven by Purkinje and Granule Cell Loss

(A) Schematic of neuroanatomical structures painted with anti-acetylated tubulin antibody at 3 days post fertilization (dpf); IT, intertectal.

(B) Representative dorsal images of acetylated tubulin immunostained larvae show that *roraa* ablation causes cerebellar defects in CRISPR/Cas9 F0 mutants and morphants. Cerebellar size was measured as indicated by the dashed red outline on inset panels.

(C) Quantification of cerebellar area in larval batches is shown for two guide (g)RNAs targeting either *roraa* exon 5 (gRNA 1) or exon 8 (gRNA 2).

(D) *roraa* morphants (injected with 3 ng morpholino; MO) display a cerebellar phenotype that can be rescued by four different wild-type *RORA* mRNA transcripts: co-injection of *roraa* e2i2 splice-blocking MO with *RORA* splice variants (*RORA* 1, GenBank: NM_134261, *RORA* 2: NM_134260, *RORA* 3: NM_002943 and *RORA* 4: NM_134262).

(E) Schematic of cerebellar cell types assessed in 3 dpf larvae using either a *neurod:egfp* transgene (green) or anti-zebrin II immunostaining (red). Orientation is indicated with A, anterior; P, posterior; L, left; R, right.

(legend continued on next page)

developing cerebellum, we deemed *roraa* as the most relevant *D. rerio* locus to test the activity of *RORA* mutations in humans.

Haploinsufficiency or knockout of *Rora* in mice lead to abnormal cerebellar layer morphology.[8,23] Therefore, to assess the effect of loss of RORA function consistent with deletion or truncating mutations identified in affected individuals, we compared the size of the developing cerebellum between *roraa* knock-down and uninjected controls. The zebrafish *roraa* locus has two annotated transcripts (GRCz10: [*roraa*-201] ENSDART00000121449.2 and [*roraa*-202] ENSDART00000148537.2), the latter of which has an incomplete 5′ coding sequence; RT-PCR using cDNA originating from 3 dpf embryos confirmed that both transcripts are detectable in this time window (Figures S6A and S6B). Next, we generated CRISPR/Cas9-based zebrafish F0 mutant models by targeting exon 5 or exon 8 of *roraa*-201 (corresponding to exon 4 or exon 7 of *roraa*-202) to produce mosaic mutants with >90% mosaicism (Figure S7). Immunostaining of the central nervous system (CNS) with anti-acetylated tubulin antibody and measurements of neuroanatomical structures showed that *roraa* F0 mutants display a reduced cerebellar area and smaller optic tecta area compared to either control larvae or larvae injected with gRNA alone ($p < 0.0001$, for gRNA 1 and gRNA 2, $n = 33–43$ and 41–45 larvae/batch, respectively, repeated, masked scoring; Figures 3A–3C and S8A–S8C).

To assess phenotype specificity and to determine the effect of *RORA* missense variants, we performed MO-mediated transient suppression of *roraa*. We designed two sb MOs targeting the splice donor site of exons 2 and 3 of *roraa*-201, which we injected into embryo batches, generated cDNA at 3 dpf, and performed RT-PCR to determine efficiency; subsequent Sanger sequencing confirmed a frameshifting deletion of *roraa* exon 2 or exon 3 (Figures S6C and S6D). Next, we injected increasing concentrations of either MO (2, 3, 4 ng e2i2; or 6, 7, 8 ng e3i3). Consistent with our CRISPR F0 mutant data, we observed a dose-dependent reduction in cerebellar size for both reagents ($p < 0.0001$, 30 to 94 larvae/condition, Figure S6E). Co-injection of e2i2 sb MO with each of the four RefSeq annotated WT human *RORA* mRNAs rescued cerebellar and optic tecta defects, indicating MO specificity ($p = 0.0060$, 0.0387, < 0.0001, < 0.0001 for *RORA* 1, 2, 3, and 4, respectively, versus MO, $n = 31–60$ larvae/batch, repeated, Figures 3B, 3D, S8A, and S8D). In parallel, heterologous expression of each of the four WT *RORA* mRNAs did not lead to cerebellar phenotypes that differed from uninjected controls ($n =$ 40–52 larvae/batch, Figure S9). To investigate further the relative expression of the four annotated *RORA* transcripts and to identify the most relevant isoform for *in vivo* modeling in zebrafish, we performed qRT-PCR on commercial human adult cDNA; we identified *RORA* 4 as the most abundantly expressed transcript in the human CNS (Figures S5A and S5B), potentially explaining the observation that WT *RORA* 4 mRNA produced the most significant restoration of cerebellar size when co-injected with MO.

Altered Purkinje and Granule Layers in *roraa* Zebrafish Models

Similar to mammals, Purkinje and granule cell crosstalk is vital for the function of the zebrafish cerebellum.[30] Cerebellar cell subpopulations have been characterized previously in zebrafish with lineage-specific markers and transgenic lines. In *neurod:egfp* transgenic zebrafish, granule cells are marked with GFP.[29] Furthermore, zebrin II is a specific marker of the Purkinje compartment,[27] which develops between 2.3 and 4 dpf.[33] To assess whether *roraa* suppression affects granule or Purkinje cell layers of zebrafish cerebellum, we conducted whole-mount zebrin II immunostaining on *neurod:egfp* transgenic zebrafish larvae at 3 dpf. F0 *roraa* mutants presented with a significantly decreased size of Purkinje and granule cell layers compared to controls ($p < 0.0001$ for both cell types; Purkinje cells, $n = 26–55$; granule cells, $n = 11–55$, repeated; Figures 3E–3H and S10A–S10C). Importantly, gRNA injected alone was indistinguishable from controls (Figures 3G and 3H). Injection of e2i2 MO recapitulated these observations ($p < 0.0001$ or $p < 0.001$ for Purkinje [$n = 29–55$] and granule [$n = 30–55$] cells, respectively, in morphants versus controls; repeated; Figures 3E–3H and S10). Further, co-injection of e2i2 MO with WT human *RORA* 4 mRNA rescued the measured area of each of the granule and Purkinje compartments ($p < 0.0001$ or $p < 0.001$ versus MO alone for Purkinje or granule cells, respectively; Figures 3E–3H and S10). Together, our data confirm that in F0 mutant or transient knockdown zebrafish models, *roraa* disruption leads to defects of Purkinje and granule cell layers, consistent with the *Rora*^{sg} mouse model.[34–36]

In Vivo Complementation Studies Indicate Dual Direction of RORA Allele Effect

To determine the pathogenicity of *RORA* missense variants (c.275G>C [p.Gly92Ala], c.281A>G [p.Lys94Arg], and c.1385G>A [p.Arg462Gln]), we assessed the effect of mutant *RORA* 4 mRNA in the presence or absence of MO.

(F) Representative dorsal images show that reduction of Purkinje and granule cells contributes to cerebellar defects induced by *roraa* targeting. Transgenic *neurod:egfp* larvae were fixed and immunostained with anti-zebrin II antibody (red), and the area comprised of each cell type was measured (as indicated in the schematic). Dashed white lines indicate measured area.
(G) Quantification of granule layer cells (GFP-positive).
(H) Quantification of Purkinje cells (zebrin II-positive). Both cell populations are reduced significantly in *roraa* F0 mutants as well as morphant zebrafish.
Scale bar in (B) and (F): 100 μm. AU, arbitrary units. Stars indicate p value compared to uninjected controls (CRISPR/Cas9 and MO) or to morphants (MO + RORA). ****$p < 0.0001$, ***$p < 0.001$, **$p < 0.01$, *$p < 0.05$; ns, not significant. Error bars in (C), (D), (G), and (H) represent the 5th and 95th percentiles.

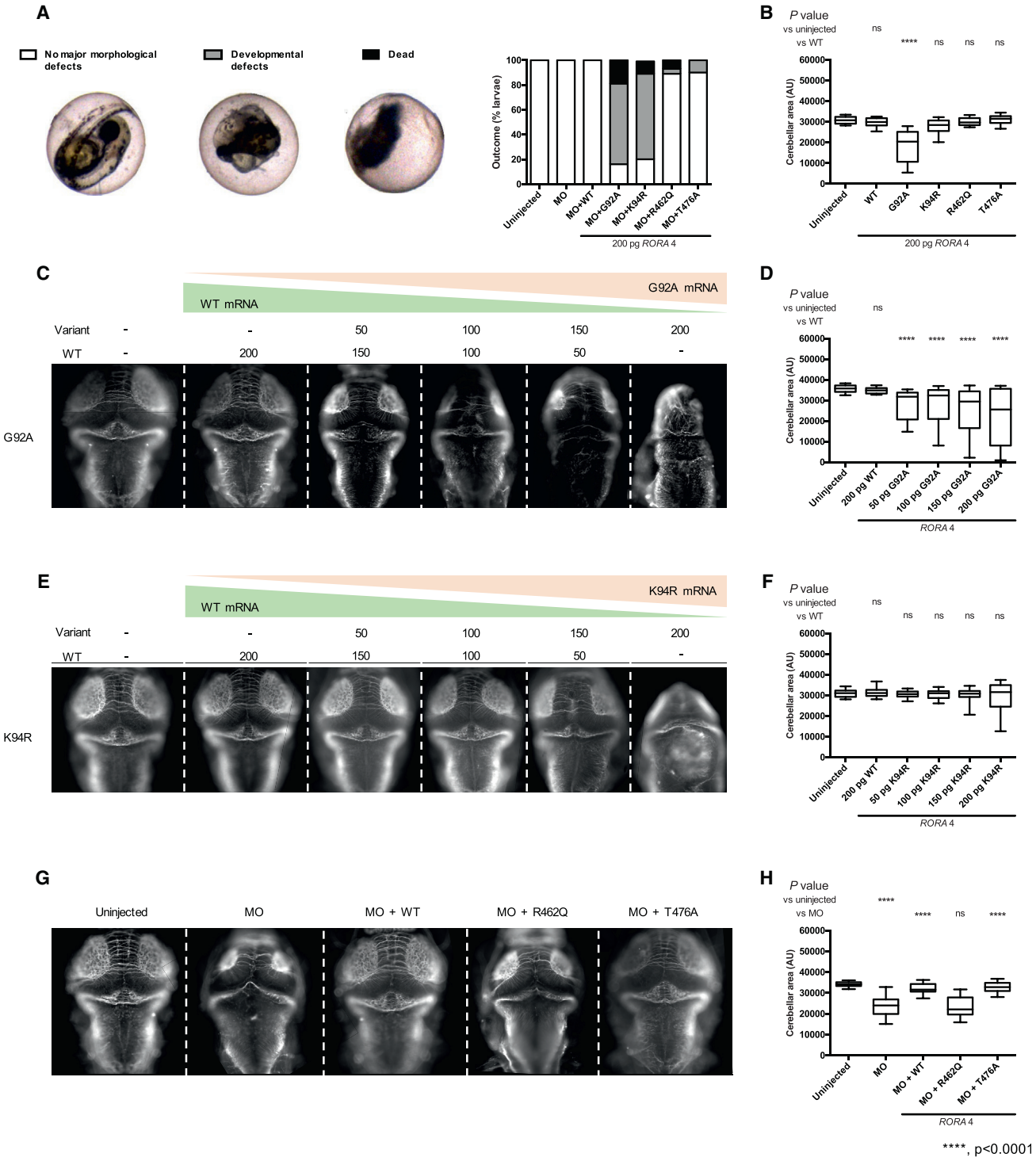

Figure 4. *RORA* Missense Variant Located in the DNA Binding Domain and Ligand Binding Domain Confer a Dominant Toxic and Loss-of-Function Effect, Respectively

(A) Complementation of *roraa* morpholino (MO) with variant mRNA results in severe gross morphological defects or larval death before 3 days post-fertilization (dpf). Left, representative embryo classes are shown; right, quantification of outcomes. p.Gly92Ala (G92A), p.Lys94Arg (K94R) are located in the DNA binding domain; p.Arg462Gln (R462Q) localizes to the ligand-binding domain; T476A (rs190933482) is a negative control for the assay with an allele frequency of 0.001091 in gnomAD).

(B) Quantification of cerebellar area of larval batches with ectopic expression of *RORA* mRNA. G92A mRNA confers a significant reduction in cerebellar size.

(C) Representative dorsal images of 3 dpf larvae injected with gradually modified doses of WT and G92A RNA (top, amount in pg) and stained with anti-acetylated tubulin antibody.

(D) Quantification of cerebellar measurements from the batches shown in (C).

(legend continued on next page)

First, we tested a loss-of-function hypothesis by co-injecting *roraa* e2i2 MO with WT or variant *RORA* 4 mRNA. *In vivo* complementation of *roraa* MO with p.Gly92Ala or p.Lys94Arg encoding mRNA resulted in early developmental defects including a reduction in the size of anterior structures and tail extension failure (65% and 69%, respectively) and a high mortality rate (19% and 10%, respectively), while co-injection of MO with p.Arg462Gln, WT, or a potentially benign variant p.Thr476Ala (rs190933482, minor allele frequency 0.001 in gnomAD) induced no appreciable morphological defects (Figure 4A). The gross morphological phenotype observed by co-injection of MO with mutant mRNAs located in the DNA binding domain was more severe than the morphant phenotype and suggested either a dominant-negative or a gain-of-function effect. To investigate these possibilities, we injected 200 pg of each mutant mRNA alone and again observed notable mortality at 3 dpf (2% for controls [1 dead larva/54] versus 31% for p.Gly92Ala [14/45]; 9% for p.Lys94Arg [4/46]; and 7% for p.Arg462Gln [3/41]). Of the larvae that survived to 3 dpf, we performed anti-acetylated immunostaining and measurement of the cerebellar area; p.Gly92Ala encoding mRNA induced a reduction in the mean cerebellar area compared to WT ($p < 0.0001$, 31–53 larvae/batch, Figure 4B). To determine whether WT mRNA could rescue the phenotypes induced by p.Gly92Ala, we titrated increasing amounts of p.Gly92Ala mRNA together with *RORA* 4 WT mRNA and observed a dose-dependent effect that correlated with the injected dose of p.Gly92Ala (Figures 4C and 4D). These data suggested a dominant toxic effect as the likely mechanism for the p.Gly92Ala variant. Although expression of p.Lys94Arg induced morphological defects similar to p.Gly92Ala and we observed a broadened distribution of cerebellar measurements at the highest dose of mutant mRNA that was consistent with p.Gly92Ala, these results did not reach statistical significance (Figures 4E and 4F). Finally, *in vivo* complementation of *roraa* MO with p.Arg462Gln encoding mRNA did not rescue the size of the cerebellum (Figures 4G and 4H, $p < 0.001$, $n = 40–41$), suggesting a loss-of-function effect as the possible disease mechanism for this change impacting the ligand binding domain (Figures 4G and 4H).

Discussion

Here, we describe a cohort of 16 affected individuals who harbor 13 different rare variants disrupting *RORA*. We observe a clinical spectrum of neurodevelopmental delay with at least two different presentations: (1) a cognitive and motor phenotype and (2) a cognitive and behavioral phenotype. The first sub-phenotype is characterized by a moderate to severe ID with a marked ataxic component, severe cerebellar vermis hypoplasia, and epilepsy with predominant generalized seizures as already reported in *RORB*,[3] whereas the hallmark of the second sub-phenotype is ASD with mild ID or normal cognition frequently associated with epilepsy. In addition to these two groups, three individuals exhibit only mild ID without behavioral problems.

Although the size of our cohort limits the delineation of an unambiguous genotype-phenotype correlation, we can infer pathomechanisms related to specific phenotypes from our *in vivo* complementation data. Individuals 2 and 3, who harbor the two dominant toxic mutations of the RORα DNA binding domain, display severe ID and motor phenotypes likely due to cerebellar hypoplasia. A similar severe phenotype is coincident with the truncating deletion (individual 6; p.Arg340Profs*17), raising the possibility that this mutation could also result in a dominant toxic effect by encoding a truncated protein; immunoblotting studies from fibroblast protein lysates showed RORA protein levels to be similar to that of controls, arguing against haploinsufficiency (Figure S4C). Individual 6 also displayed autistic traits, but these phenotypes occurred secondary to established ID, potentially excluding her from the Autism Diagnosis Interview (ADI) criteria for idiopathic ASD.[37,38]

By contrast, we note variability in cognitive function and behavioral phenotypes in individuals with likely haploinsufficiency. One individual displays an ASD phenotype in the absence of ID (individual 8), and *in vivo* complementation testing in zebrafish indicate that the p.Arg462Gln mutation confers a loss-of-function effect. Further, 6/12 individuals from simplex families who likely have a reduction in protein dosage display mild to moderate ID but with normal behavior, while the remaining 5/12 affected individuals from simplex families present with both ID and autistic features. Notably, there is phenotypic variability among the individuals within multiplex family 10: all four individuals display mild ID, but only two display behavioral anomalies. However, we cannot exclude the possibility of *trans* effects from elsewhere in the genome, especially from *DISC1* affected by the CNVs harbored by individuals 10A–C or individual 11 (Figure S1; Table S4). Phenotypic variability is not uncommon for neurodevelopmental disorders,[39] and here

(E) Representative dorsal images of 3 dpf larvae injected with gradually modified doses of WT and K94R RNA (top, amount in pg) and stained with anti-acetylated tubulin antibody.
(F) Quantification of cerebellar measurements from the batches shown in (E).
(G) Representative dorsal images of 3 dpf larvae injected either with e2i2 splice-blocking MO or MO co-injected with WT *RORA* mRNA, R462Q or population control T476A variant *RORA* mRNA.
(H) Quantification of cerebellar measurements from the batches shown in (E).
AU, arbitrary units. Stars indicate p value compared to WT. ****$p < 0.0001$; ns, not significant. Error bars in (B), (D), (F), and (H) represent the 5^{th} and 95^{th} percentiles.

we account, in part, for variability due to allelism at the *RORA* locus by elucidating the direction of allele effect for missense changes.

The sub-group of our cohort who show a constellation of cognitive and motor defects are reminiscent of the homozygous *staggerer* (*sg/sg*) mouse, an early reported animal model of *Rora* ablation. The *staggerer* mutation consists of an intragenic CNV that results in a 122-bp frameshifting deletion that truncates the ligand binding domain, leading to the loss of RORα activity.[8] This phenotype is similar to $Rora^{-/-}$ mice[40] in which the most obvious symptom is an ataxic gait associated with defective Purkinje cell development leading to an abnormal cerebellar size.[41] Heterozygous $Rora^{+/-}$ mice present with a comparable phenotype, although they display a late onset of neuronal loss and reduced phenotypic severity.[42] Further studies will be required to understand the precise molecular mechanisms of p.Gly92Ala and p.Lys94Arg to account for their apparent toxic effects. We speculate that these changes in the DNA binding domain might hamper access of WT RORα to its natural target sites (Figure S3B), thereby leading to a phenotype resembling to the *staggerer* and $Rora^{-/-}$ homozygous mutants.

The autistic signs observed in two individuals with truncating mutations (individuals 6 and 13) and two individuals with missense mutations altering the ligand binding domain of *RORA* (individuals 7 and 8) are in agreement with recent reports suggesting that *RORA* is a candidate gene for ASD.[43] ChIP-on-chip analysis has revealed that RORα can be recruited to the promoter regions of 2,544 genes across the human genome, with a significant enrichment in biological functions including neuronal differentiation, adhesion, and survival, synaptogenesis, synaptic transmission and plasticity, and axonogenesis, as well as higher-level functions such as development of the cortex and cerebellum, cognition, memory, and spatial learning.[44] Independent ChIP-quantitative PCR analyses confirmed binding of RORA to promoter regions of selected ASD-associated genes, including *A2BP1*, *CYP19A1*, *ITPR1*, *NLGN1*, and *NTRK2*, whose expression levels are also decreased in *RORA*-repressed human neuronal cells and in prefrontal cortex tissues from individuals with ASD.[44] Additionally, two *RORA* polymorphisms (rs11639084 and rs4774388) have been associated with ASD risk in Iranian individuals.[45] Consistent with these data, treatment with a synthetic RORα/γ agonist, SR1078, reduced repetitive behavior in the BTBR mouse model of autism, suggesting that *RORA* upregulation could be a viable therapeutic option for ASD.[46]

In summary, our data implicate a diverse series of disruptive mutations in *RORA* with neurological phenotypes hallmarked by ID and either severe motor phenotypes or behavioral anomalies. Through combined clinical, genetic, and functional studies, we expand the genetic basis of rare neurodevelopmental syndromes and show how *in vivo* modeling can reveal dual molecular mutational effects.

Supplemental Data

Supplemental Data include ten figures and four tables and can be found with this article online at https://doi.org/10.1016/j.ajhg.2018.02.021.

Acknowledgments

We are grateful to Dr. R. Hawkes and Dr. C. Armstrong (University of Calgary) for providing the zebrin II antibody. We also thank Mr. Z. Kupchinsky for zebrafish husbandry, Mr. D. Morrow for assisting with reagents for the *in vivo* modeling study, and members of the Center for Human Disease Modeling for helpful comments. We are also grateful to Ms. J.A. Rosenfeld (Mokry) for her precious help in our search for similar affected individuals and for her review of the manuscript. This work was supported by funds from the Agence Nationale pour la Recherche/E-rare Joint-Transnational-Call 2011 (2011-RARE-004-01 "Euro-SCAR") to M.K.; from the National Human Genome Research Institute with supplemental funding provided by the National Heart, Lung, and Blood Institute under the Trans-Omics for Precision Medicine (TOPMed) program and the National Eye Institute (to the Broad Center for Mendelian Genomics [UM1 HG008900]); from the NIH grant T32 HD07466 (to M.H.W.); US NIH grant R01 MH106826 to E.E.D.; and from the Estonian Research Council, grant PUT355 (to S.P. and K.Õ.). We also acknowledge the Deciphering Developmental Disorders (DDD) Study.

K.M., M.T.C., R.W., M.J.G.S., and K.R. are employees of GeneDx, Inc., a wholly owned subsidiary of OPKO Health, Inc. N.K. is a paid consultant for and holds significant stock of Rescindo Therapeutics, Inc.

Received: December 18, 2017
Accepted: February 26, 2018
Published: April 12, 2018

Web Resources

1000 Genomes, http://www.internationalgenome.org/
CHOPCHOP, http://chopchop.cbu.uib.no/
Clustal: Multiple Sequence Alignment, http://www.clustal.org/
Database of Genomic Variants (DGV), http://dgv.tcag.ca/dgv/app/home
DECIPHER, https://decipher.sanger.ac.uk/
dbSNP, https://www.ncbi.nlm.nih.gov/projects/SNP/
Ensembl Genome Browser, http://www.ensembl.org/index.html
ExAC Browser, http://exac.broadinstitute.org/
GenBank, https://www.ncbi.nlm.nih.gov/genbank/
GeneMatcher, https://genematcher.org/
gnomAD Browser, http://gnomad.broadinstitute.org/
ImageJ Fiji, http://fiji.sc/Fiji
NHLBI Exome Sequencing Project (ESP) Exome Variant Server, http://evs.gs.washington.edu/EVS/
OMIM, http://www.omim.org/
PLINK, https://www.partners.org/~purcell/plink/
QuickChange Primer Design, https://www.genomics.agilent.com/primerDesignProgram.jsp
seqr, https://seqr.broadinstitute.org/
The Human Protein Atlas, http://www.proteinatlas.org/
UCSC Genome Browser, http://genome.ucsc.edu
UniProt, http://www.uniprot.org/
ZFIN, http://zfin.org

References

1. Escriva, H., Langlois, M.C., Mendonça, R.L., Pierce, R., and Laudet, V. (1998). Evolution and diversification of the nuclear receptor superfamily. Ann. N Y Acad. Sci. *839*, 143–146.
2. Sladek, F.M. (2011). What are nuclear receptor ligands? Mol. Cell. Endocrinol. *334*, 3–13.
3. Rudolf, G., Lesca, G., Mehrjouy, M.M., Labalme, A., Salmi, M., Bache, I., Bruneau, N., Pendziwiat, M., Fluss, J., de Bellescize, J., et al. (2016). Loss of function of the retinoid-related nuclear receptor (RORB) gene and epilepsy. Eur. J. Hum. Genet. *24*, 1761–1770.
4. Okada, S., Markle, J.G., Deenick, E.K., Mele, F., Averbuch, D., Lagos, M., Alzahrani, M., Al-Muhsen, S., Halwani, R., Ma, C.S., et al. (2015). IMMUNODEFICIENCIES. Impairment of immunity to *Candida* and *Mycobacterium* in humans with bi-allelic RORC mutations. Science *349*, 606–613.
5. Bardoni, B., Zanaria, E., Guioli, S., Floridia, G., Worley, K.C., Tonini, G., Ferrante, E., Chiumello, G., McCabe, E.R., Fraccaro, M., et al. (1994). A dosage sensitive locus at chromosome Xp21 is involved in male to female sex reversal. Nat. Genet. *7*, 497–501.
6. Muscatelli, F., Strom, T.M., Walker, A.P., Zanaria, E., Récan, D., Meindl, A., Bardoni, B., Guioli, S., Zehetner, G., Rabl, W., et al. (1994). Mutations in the DAX-1 gene give rise to both X-linked adrenal hypoplasia congenita and hypogonadotropic hypogonadism. Nature *372*, 672–676.
7. Giguère, V., Tini, M., Flock, G., Ong, E., Evans, R.M., and Otulakowski, G. (1994). Isoform-specific amino-terminal domains dictate DNA-binding properties of ROR alpha, a novel family of orphan hormone nuclear receptors. Genes Dev. *8*, 538–553.
8. Hamilton, B.A., Frankel, W.N., Kerrebrock, A.W., Hawkins, T.L., FitzHugh, W., Kusumi, K., Russell, L.B., Mueller, K.L., van Berkel, V., Birren, B.W., et al. (1996). Disruption of the nuclear hormone receptor RORalpha in staggerer mice. Nature *379*, 736–739.
9. Yamamoto, T., Mencarelli, M.A., Di Marco, C., Mucciolo, M., Vascotto, M., Balestri, P., Gérard, M., Mathieu-Dramard, M., Andrieux, J., Breuning, M., et al. (2014). Overlapping microdeletions involving 15q22.2 narrow the critical region for intellectual disability to NARG2 and RORA. Eur. J. Med. Genet. *57*, 163–168.
10. Boutry-Kryza, N., Labalme, A., Till, M., Schluth-Bolard, C., Langue, J., Turleau, C., Edery, P., and Sanlaville, D. (2012). An 800 kb deletion at 17q23.2 including the MED13 (THRAP1) gene, revealed by aCGH in a patient with a SMC 17p. Am. J. Med. Genet. A. *158A*, 400–405.
11. Grønborg, S., Kjaergaard, S., Hove, H., Larsen, V.A., and Kirchhoff, M. (2015). Monozygotic twins with a de novo 0.32cMb 16q24.3 deletion, including TUBB3 presenting with developmental delay and mild facial dysmorphism but without overt brain malformation. Am. J. Med. Genet. A. *167A*, 2731–2736.
12. Sali, A., and Blundell, T.L. (1993). Comparative protein modelling by satisfaction of spatial restraints. J. Mol. Biol. *234*, 779–815.
13. Obholzer, N., Wolfson, S., Trapani, J.G., Mo, W., Nechiporuk, A., Busch-Nentwich, E., Seiler, C., Sidi, S., Söllner, C., Duncan, R.N., et al. (2008). Vesicular glutamate transporter 3 is required for synaptic transmission in zebrafish hair cells. J. Neurosci. *28*, 2110–2118.
14. Montague, T.G., Cruz, J.M., Gagnon, J.A., Church, G.M., and Valen, E. (2014). CHOPCHOP: a CRISPR/Cas9 and TALEN web tool for genome editing. Nucleic Acids Res. *42*, W401-7.
15. Küry, S., Besnard, T., Ebstein, F., Khan, T.N., Gambin, T., Douglas, J., Bacino, C.A., Craigen, W.J., Sanders, S.J., Lehmann, A., et al. (2017). De novo disruption of the proteasome regulatory subunit PSMD12 causes a syndromic neurodevelopmental disorder. Am. J. Hum. Genet. *100*, 352–363.
16. Stankiewicz, P., Khan, T.N., Szafranski, P., Slattery, L., Streff, H., Vetrini, F., Bernstein, J.A., Brown, C.W., Rosenfeld, J.A., Rednam, S., et al.; Deciphering Developmental Disorders Study (2017). Haploinsufficiency of the chromatin remodeler BPTF causes syndromic developmental and speech delay, postnatal microcephaly, and dysmorphic features. Am. J. Hum. Genet. *101*, 503–515.
17. Ta-Shma, A., Khan, T.N., Vivante, A., Willer, J.R., Matak, P., Jalas, C., Pode-Shakked, B., Salem, Y., Anikster, Y., Hildebrandt, F., et al. (2017). Mutations in TMEM260 cause a pediatric neurodevelopmental, cardiac, and renal syndrome. Am. J. Hum. Genet. *100*, 666–675.
18. Niederriter, A.R., Davis, E.E., Golzio, C., Oh, E.C., Tsai, I.-C., and Katsanis, N. (2013). In vivo modeling of the morbid human genome using Danio rerio. J. Vis. Exp., e50338.
19. Margolin, D.H., Kousi, M., Chan, Y.-M., Lim, E.T., Schmahmann, J.D., Hadjivassiliou, M., Hall, J.E., Adam, I., Dwyer, A., Plummer, L., et al. (2013). Ataxia, dementia, and hypogonadotropism caused by disordered ubiquitination. N. Engl. J. Med. *368*, 1992–2003.
20. Schneider, C.A., Rasband, W.S., and Eliceiri, K.W. (2012). NIH Image to ImageJ: 25 years of image analysis. Nat. Methods *9*, 671–675.
21. Sobreira, N., Schiettecatte, F., Valle, D., and Hamosh, A. (2015). GeneMatcher: a matching tool for connecting investigators with an interest in the same gene. Hum. Mutat. *36*, 928–930.
22. Ruff, M., Gangloff, M., Wurtz, J.M., and Moras, D. (2000). Estrogen receptor transcription and transactivation: Structure-function relationship in DNA- and ligand-binding domains of estrogen receptors. Breast Cancer Res. *2*, 353–359.
23. Sidman, R.L., Lane, P.W., and Dickie, M.M. (1962). Staggerer, a new mutation in the mouse affecting the cerebellum. Science *137*, 610–612.
24. Marin-Valencia, I., Novarino, G., Johansen, A., Rosti, B., Issa, M.Y., Musaev, D., Bhat, G., Scott, E., Silhavy, J.L., Stanley, V., et al. (2018). A homozygous founder mutation in*TRAPPC6B* associates with a neurodevelopmental disorder characterised by microcephaly, epilepsy and autistic features. J. Med. Genet. *55*, 48–54.
25. Schaffer, A.E., Eggens, V.R.C., Caglayan, A.O., Reuter, M.S., Scott, E., Coufal, N.G., Silhavy, J.L., Xue, Y., Kayserili, H., Yasuno, K., et al. (2014). CLP1 founder mutation links tRNA splicing and maturation to cerebellar development and neurodegeneration. Cell *157*, 651–663.
26. Borck, G., Hög, F., Dentici, M.L., Tan, P.L., Sowada, N., Medeira, A., Gueneau, L., Thiele, H., Kousi, M., Lepri, F., et al. (2015). BRF1 mutations alter RNA polymerase III-dependent transcription and cause neurodevelopmental anomalies. Genome Res. *25*, 155–166.
27. Akizu, N., Cantagrel, V., Zaki, M.S., Al-Gazali, L., Wang, X., Rosti, R.O., Dikoglu, E., Gelot, A.B., Rosti, B., Vaux, K.K., et al. (2015). Biallelic mutations in SNX14 cause a syndromic form of cerebellar atrophy and lysosome-autophagosome dysfunction. Nat. Genet. *47*, 528–534.

28. Frosk, P., Arts, H.H., Philippe, J., Gunn, C.S., Brown, E.L., Chodirker, B., Simard, L., Majewski, J., Fahiminiya, S., Russell, C., et al.; FORGE Canada Consortium; and Canadian Rare Diseases: Models & Mechanisms Network (2017). A truncating mutation in CEP55 is the likely cause of MARCH, a novel syndrome affecting neuronal mitosis. J. Med. Genet. *54*, 490–501.
29. Anttonen, A.-K., Laari, A., Kousi, M., Yang, Y.J., Jääskeläinen, T., Somer, M., Siintola, E., Jakkula, E., Muona, M., Tegelberg, S., et al. (2017). ZNHIT3 is defective in PEHO syndrome, a severe encephalopathy with cerebellar granule neuron loss. Brain *140*, 1267–1279.
30. Hibi, M., and Shimizu, T. (2012). Development of the cerebellum and cerebellar neural circuits. Dev. Neurobiol. *72*, 282–301.
31. Bertrand, S., Thisse, B., Tavares, R., Sachs, L., Chaumot, A., Bardet, P.-L., Escrivà, H., Duffraisse, M., Marchand, O., Safi, R., et al. (2007). Unexpected novel relational links uncovered by extensive developmental profiling of nuclear receptor expression. PLoS Genet. *3*, e188.
32. Katsuyama, Y., Oomiya, Y., Dekimoto, H., Motooka, E., Takano, A., Kikkawa, S., Hibi, M., and Terashima, T. (2007). Expression of zebrafish ROR alpha gene in cerebellar-like structures. Dev. Dyn *236*, 2694–2701.
33. Hamling, K.R., Tobias, Z.J.C., and Weissman, T.A. (2015). Mapping the development of cerebellar Purkinje cells in zebrafish. Dev. Neurobiol. *75*, 1174–1188.
34. Gold, D.A., Gent, P.M., and Hamilton, B.A. (2007). ROR alpha in genetic control of cerebellum development: 50 staggering years. Brain Res. *1140*, 19–25.
35. Vogel, M.W., Sinclair, M., Qiu, D., and Fan, H. (2000). Purkinje cell fate in staggerer mutants: agenesis versus cell death. J. Neurobiol. *42*, 323–337.
36. Yoon, C.H. (1972). Developmental mechanism for changes in cerebellum of "staggerer" mouse, a neurological mutant of genetic origin. Neurology *22*, 743–754.
37. Tammimies, K., Marshall, C.R., Walker, S., Kaur, G., Thiruvahindrapuram, B., Lionel, A.C., Yuen, R.K.C., Uddin, M., Roberts, W., Weksberg, R., et al. (2015). Molecular diagnostic yield of chromosomal microarray analysis and whole-exome sequencing in children with autism spectrum disorder. JAMA *314*, 895–903.
38. Chérot, E., Keren, B., Dubourg, C., Carré, W., Fradin, M., Lavillaureix, A., Afenjar, A., Burglen, L., Whalen, S., Charles, P., et al. (2018). Using medical exome sequencing to identify the causes of neurodevelopmental disorders: Experience of 2 clinical units and 216 patients. Clin. Genet. *93*, 567–576.
39. Hu, W.F., Chahrour, M.H., and Walsh, C.A. (2014). The diverse genetic landscape of neurodevelopmental disorders. Annu. Rev. Genomics Hum. Genet. *15*, 195–213.
40. Doulazmi, M., Frédéric, F., Capone, F., Becker-André, M., Delhaye-Bouchaud, N., and Mariani, J. (2001). A comparative study of Purkinje cells in two RORalpha gene mutant mice: staggerer and RORalpha(-/-). Brain Res. Dev. Brain Res. *127*, 165–174.
41. Herrup, K., Shojaeian-Zanjani, H., Panzini, L., Sunter, K., and Mariani, J. (1996). The numerical matching of source and target populations in the CNS: the inferior olive to Purkinje cell projection. Brain Res. Dev. Brain Res. *96*, 28–35.
42. Doulazmi, M., Capone, F., Frederic, F., Bakouche, J., Lemaigre-Dubreuil, Y., and Mariani, J. (2006). Cerebellar purkinje cell loss in heterozygous rora+/- mice: a longitudinal study. J. Neurogenet. *20*, 1–17.
43. Nguyen, A., Rauch, T.A., Pfeifer, G.P., and Hu, V.W. (2010). Global methylation profiling of lymphoblastoid cell lines reveals epigenetic contributions to autism spectrum disorders and a novel autism candidate gene, RORA, whose protein product is reduced in autistic brain. FASEB J. *24*, 3036–3051.
44. Sarachana, T., and Hu, V.W. (2013). Genome-wide identification of transcriptional targets of RORA reveals direct regulation of multiple genes associated with autism spectrum disorder. Mol. Autism *4*, 14.
45. Sayad, A., Noroozi, R., Omrani, M.D., Taheri, M., and Ghafouri-Fard, S. (2017). Retinoic acid-related orphan receptor alpha (RORA) variants are associated with autism spectrum disorder. Metab. Brain Dis. *32*, 1595–1601.
46. Wang, Y., Billon, C., Walker, J.K., and Burris, T.P. (2016). Therapeutic effect of a synthetic RORα/γ agonist in an animal model of autism. ACS Chem. Neurosci. *7*, 143–148.

The American Journal of Human Genetics, Volume *102*

Supplemental Data

Dual Molecular Effects of Dominant *RORA* Mutations Cause Two Variants of Syndromic Intellectual Disability with Either Autism or Cerebellar Ataxia

Claire Guissart, Xenia Latypova, Paul Rollier, Tahir N. Khan, Hannah Stamberger, Kirsty McWalter, Megan T. Cho, Susanne Kjaergaard, Sarah Weckhuysen, Gaetan Lesca, Thomas Besnard, Katrin Õunap, Lynn Schema, Andreas G. Chiocchetti, Marie McDonald, Julitta de Bellescize, Marie Vincent, Hilde Van Esch, Shannon Sattler, Irman Forghani, Isabelle Thiffault, Christine M. Freitag, Deborah Sara Barbouth, Maxime Cadieux-Dion, Rebecca Willaert, Maria J. Guillen Sacoto, Nicole P. Safina, Christèle Dubourg, Lauren Grote, Wilfrid Carré, Carol Saunders, Sander Pajusalu, Emily Farrow, Anne Boland, Danielle Hays Karlowicz, Jean-François Deleuze, Monica H. Wojcik, Rena Pressman, Bertrand Isidor, Annick Vogels, Wim Van Paesschen, Lihadh Al-Gazali, Aisha Mohamed Al Shamsi, Mireille Claustres, Aurora Pujol, Stephan J. Sanders, François Rivier, Nicolas Leboucq, Benjamin Cogné, Souphatta Sasorith, Damien Sanlaville, Kyle Retterer, Sylvie Odent, Nicholas Katsanis, Stéphane Bézieau, Michel Koenig, Erica E. Davis, Laurent Pasquier, and Sébastien Küry

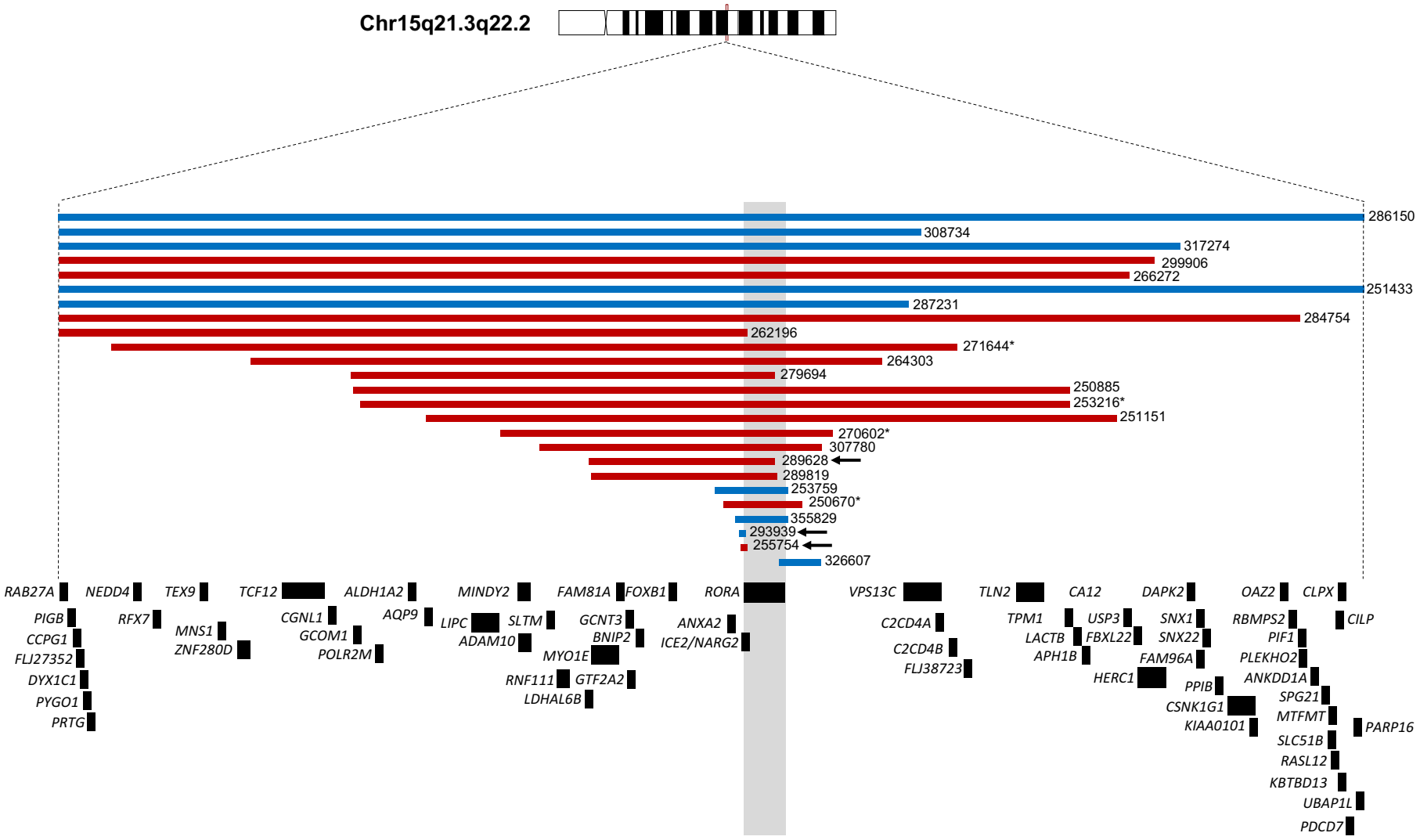
Chr15q21.3q22.2
286150
308734
317274
299906
266272
251433
287231
284754
262196
271644*
264303
279694
250885
253216*
251151
270602*
307780
289628
289819
253759
250670*
355829
293939
255754
326607
RAB27A
NEDD4
TEX9
TCF12
ALDH1A2
MINDY2
FAM81A
FOXB1
RORA
VPS13C
TLN2
CA12
DAPK2
OAZ2
CLPX
PIGB
RFX7
CGNL1
AQP9
LIPC
SLTM
GCNT3
ANXA2
C2CD4A
TPM1
USP3
SNX1
RBMPS2
CILP
CCPG1
MNS1
GCOM1
ADAM10
BNIP2
ICE2/NARG2
C2CD4B
LACTB
FBXL22
SNX22
PIF1
FLJ27352
ZNF280D
POLR2M
MYO1E
FLJ38723
APH1B
FAM96A
PLEKHO2
DYX1C1
RNF111
GTF2A2
HERC1
ANKDD1A
PYGO1
LDHAL6B
PPIB
SPG21
PRTG
CSNK1G1
MTFMT
PARP16
KIAA0101
SLC51B
RASL12
KBTBD13
UBAP1L
PDCD7

Figure S1

Figure S1. Schematic of copy number variants in the DECIPHER database encompassing the *RORA* locus on 15q22. Copy number loss (deletion) is shown in red; copy number gain (duplication) is shown in blue. DECIPHER individual case numbers are provided. Individuals included in our study are marked by arrows, and individuals reported previously (Yamamoto et al., 2014) are indicated by asterisks. Vertical gray shaded bar indicates the *RORA* locus. Database query was conducted in December 2017.

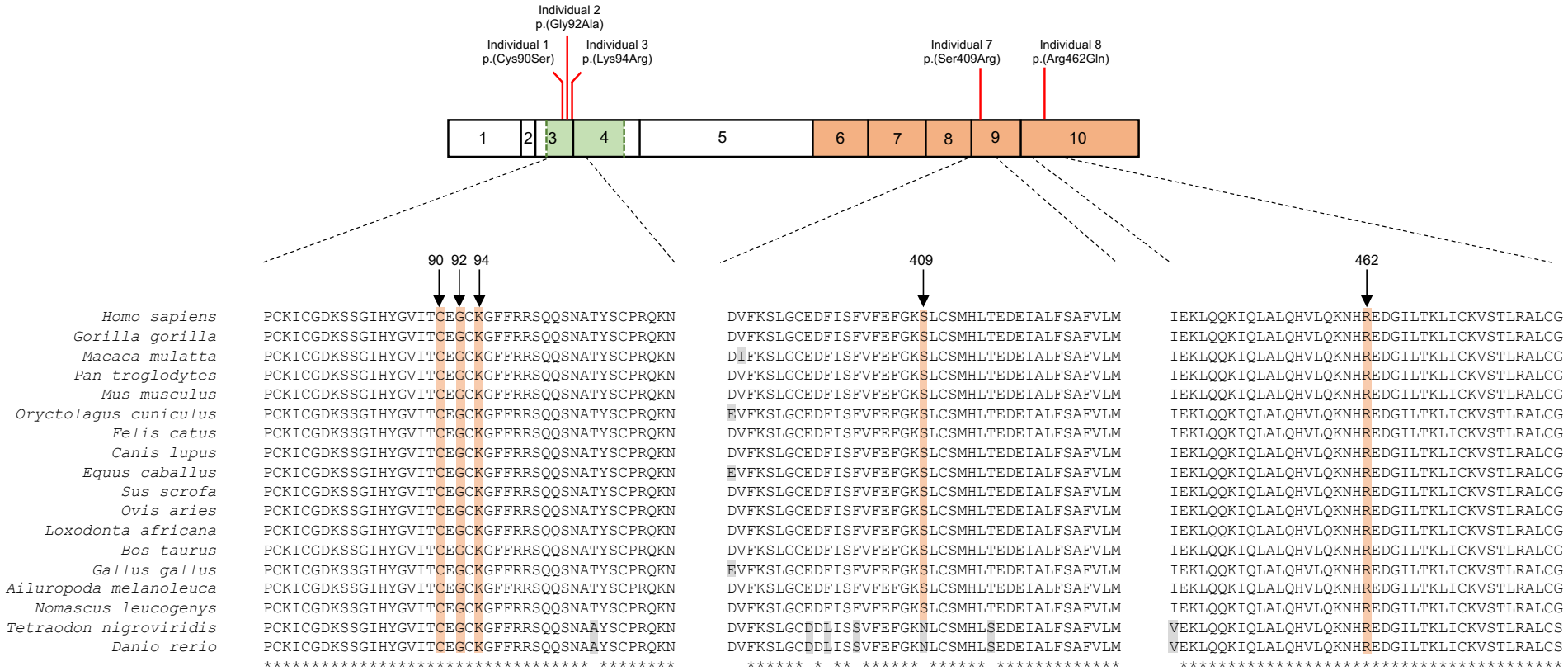
Individual 2
p.(Gly92Ala)
Individual 1
p.(Cys90Ser)
Individual 3
p.(Lys94Arg)
Individual 7
p.(Ser409Arg)
Individual 8
p.(Arg462Gln)
1
2
3
4
5
6
7
8
9
10
90 92 94
409
462
Homo sapiens PCKICGDKSSGIHYGVITCEGCKGFFRRSQQSNATYSCPRQKN DVFKSLGCEDFISFVFEFGKSLCSMHLTEDEIALFSAFVLM IEKLQQKIQLALQHVLQKNHREDGILTKLICKVSTLRALCG
Gorilla gorilla PCKICGDKSSGIHYGVITCEGCKGFFRRSQQSNATYSCPRQKN DVFKSLGCEDFISFVFEFGKSLCSMHLTEDEIALFSAFVLM IEKLQQKIQLALQHVLQKNHREDGILTKLICKVSTLRALCG
Macaca mulatta PCKICGDKSSGIHYGVITCEGCKGFFRRSQQSNATYSCPRQKN DIFKSLGCEDFISFVFEFGKSLCSMHLTEDEIALFSAFVLM IEKLQQKIQLALQHVLQKNHREDGILTKLICKVSTLRALCG
Pan troglodytes PCKICGDKSSGIHYGVITCEGCKGFFRRSQQSNATYSCPRQKN DVFKSLGCEDFISFVFEFGKSLCSMHLTEDEIALFSAFVLM IEKLQQKIQLALQHVLQKNHREDGILTKLICKVSTLRALCG
Mus musculus PCKICGDKSSGIHYGVITCEGCKGFFRRSQQSNATYSCPRQKN DVFKSLGCEDFISFVFEFGKSLCSMHLTEDEIALFSAFVLM IEKLQQKIQLALQHVLQKNHREDGILTKLICKVSTLRALCG
Oryctolagus cuniculus PCKICGDKSSGIHYGVITCEGCKGFFRRSQQSNATYSCPRQKN EVFKSLGCEDFISFVFEFGKSLCSMHLTEDEIALFSAFVLM IEKLQQKIQLALQHVLQKNHREDGILTKLICKVSTLRALCG
Felis catus PCKICGDKSSGIHYGVITCEGCKGFFRRSQQSNATYSCPRQKN DVFKSLGCEDFISFVFEFGKSLCSMHLTEDEIALFSAFVLM IEKLQQKIQLALQHVLQKNHREDGILTKLICKVSTLRALCG
Canis lupus PCKICGDKSSGIHYGVITCEGCKGFFRRSQQSNATYSCPRQKN DVFKSLGCEDFISFVFEFGKSLCSMHLTEDEIALFSAFVLM IEKLQQKIQLALQHVLQKNHREDGILTKLICKVSTLRALCG
Equus caballus PCKICGDKSSGIHYGVITCEGCKGFFRRSQQSNATYSCPRQKN EVFKSLGCEDFISFVFEFGKSLCSMHLTEDEIALFSAFVLM IEKLQQKIQLALQHVLQKNHREDGILTKLICKVSTLRALCG
Sus scrofa PCKICGDKSSGIHYGVITCEGCKGFFRRSQQSNATYSCPRQKN DVFKSLGCEDFISFVFEFGKSLCSMHLTEDEIALFSAFVLM IEKLQQKIQLALQHVLQKNHREDGILTKLICKVSTLRALCG
Ovis aries PCKICGDKSSGIHYGVITCEGCKGFFRRSQQSNATYSCPRQKN DVFKSLGCEDFISFVFEFGKSLCSMHLTEDEIALFSAFVLM IEKLQQKIQLALQHVLQKNHREDGILTKLICKVSTLRALCG
Loxodonta africana PCKICGDKSSGIHYGVITCEGCKGFFRRSQQSNATYSCPRQKN DVFKSLGCEDFISFVFEFGKSLCSMHLTEDEIALFSAFVLM IEKLQQKIQLALQHVLQKNHREDGILTKLICKVSTLRALCG
Bos taurus PCKICGDKSSGIHYGVITCEGCKGFFRRSQQSNATYSCPRQKN DVFKSLGCEDFISFVFEFGKSLCSMHLTEDEIALFSAFVLM IEKLQQKIQLALQHVLQKNHREDGILTKLICKVSTLRALCG
Gallus gallus PCKICGDKSSGIHYGVITCEGCKGFFRRSQQSNATYSCPRQKN EVFKSLGCEDFISFVFEFGKSLCSMHLTEDEIALFSAFVLM IEKLQQKIQLALQHVLQKNHREDGILTKLICKVSTLRALCG
Ailuropoda melanoleuca PCKICGDKSSGIHYGVITCEGCKGFFRRSQQSNATYSCPRQKN DVFKSLGCEDFISFVFEFGKSLCSMHLTEDEIALFSAFVLM IEKLQQKIQLALQHVLQKNHREDGILTKLICKVSTLRALCG
Nomascus leucogenys PCKICGDKSSGIHYGVITCEGCKGFFRRSQQSNATYSCPRQKN DVFKSLGCEDFISFVFEFGKSLCSMHLTEDEIALFSAFVLM IEKLQQKIQLALQHVLQKNHREDGILTKLICKVSTLRALCG
Tetraodon nigroviridis PCKICGDKSSGIHYGVITCEGCKGFFRRSQQSNAAYSCPRQKN DVFKSLGCDDLISSVFEFGKNLCSMHLSEDEIALFSAFVLM VEKLQQKIQLALQHVLQKNHREDGILTKLICKVSTLRALCS
Danio rerio PCKICGDKSSGIHYGVITCEGCKGFFRRSQQSNAAYSCPRQKN DVFKSLGCDDLISSVFEFGKNLCSMHLSEDEIALFSAFVLM VEKLQQKIQLALQHVLQKNHREDGILTKLICKVSTLRALCS

Figure S2

Figure S2. Multiple protein sequence alignment of RORA orthologs across vertebrate species show conservation of missense mutations detected in cases. Schematic of the RORa protein (NP_599023.1) and its domains (DNA binding domain, green; ligand binding domain, orange) and location of each of the missense variants reported in this study (top). Protein sequence alignments from 18 vertebrate species is shown (bottom). Orange shading in the alignment indicates RORA amino acids Cys90, Gly92, Lys94, Ser409, and Arg462. Grey shading indicates species-specific non-conserved amino acids. Asterisk indicates 100% conservation across mentioned species. Multiple sequence alignment was performed with ClustalW using the following UniProt identifiers: P35398, *Homo sapiens*; G3QE47, *Gorilla gorilla*; F7E9K9, *Macaca mulatta*; H2R8C9, *Pan troglodytes*; P51448, *Mus musculus*; G1T4B2, *Oryctolagus cuniculus*; M3WJ80, *Felis catus*; F1P607, *Canis lupus*; F6X794, *Equus caballus*; F1S075, *Sus scrofa*; W5QI24, *Ovis aries*; G3SLZ5, *Loxodonta africana*; F1N7R0, *Bos taurus*; F1NML9, *Gallus gallus*; G1LN19, *Ailuropoda melanoleuca*; G1RMH6, *Nomascus leucogenys*; H3CSJ1, *Tetraodon nigroviridis*; A7VL70, *Danio rerio*.

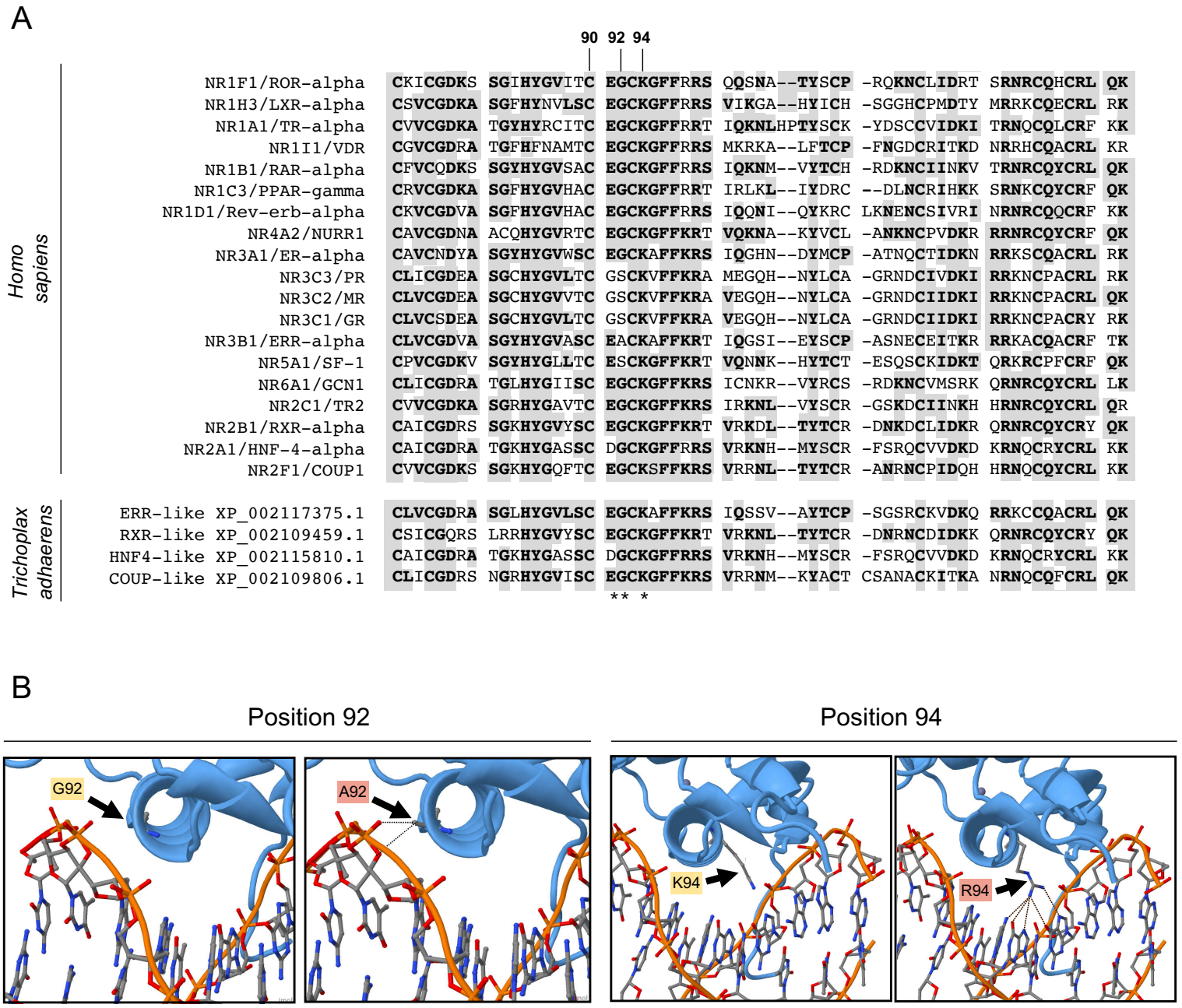
A
90 92 94
Homo sapiens
NR1F1/ROR-alpha CKICGDKS SGIHYGVITC EGCKGFFRRS QQSNA--TYSCP -RQKNCLIDRT SRNRCQHCRL QK
NR1H3/LXR-alpha CSVCGDKA SGFHYNVLSC EGCKGFFRRS VIKGA--HYICH -SGGHCPMDTY MRRKCQECRL RK
NR1A1/TR-alpha CVVCGDKA TGYHYRCITC EGCKGFFRRT IQKNLHPTYSCK -YDSCCVIDKI TRNQCQLCRF KK
NR1I1/VDR CGVCGDRA TGFHFNAMTC EGCKGFFRRS MKRKA--LFTCP -FNGDCRITKD NRRHCQACRL KR
NR1B1/RAR-alpha CFVCQDKS SGYHYGVSAC EGCKGFFRRS IQKNM--VYTCH -RDKNCIINKV TRNRCQYCRL QK
NR1C3/PPAR-gamma CRVCGDKA SGFHYGVHAC EGCKGFFRRT IRLKL--IYDRC --DLNCRIHKK SRNKCQYCRF QK
NR1D1/Rev-erb-alpha CKVCGDVA SGFHYGVHAC EGCKGFFRRS IQQNI--QYKRC LKNENCSIVRI NRNRCQQCRF KK
NR4A2/NURR1 CAVCGDNA ACQHYGVRTC EGCKGFFKRT VQKNA--KYVCL -ANKNCPVDKR RRNRCQYCRF QK
NR3A1/ER-alpha CAVCNDYA SGYHYGVWSC EGCKAFFKRS IQGHN--DYMCP -ATNQCTIDKN RRKSCQACRL RK
NR3C3/PR CLICGDEA SGCHYGVLTC GSCKVFFKRA MEGQH--NYLCA -GRNDCIVDKI RRKNCPACRL RK
NR3C2/MR CLVCGDEA SGCHYGVVTC GSCKVFFKRA VEGQH--NYLCA -GRNDCIIDKI RRKNCPACRL QK
NR3C1/GR CLVCSDEA SGCHYGVLTC GSCKVFFKRA VEGQH--NYLCA -GRNDCIIDKI RRKNCPACRY RK
NR3B1/ERR-alpha CLVCGDVA SGYHYGVASC EACKAFFKRT IQGSI--EYSCP -ASNECEITKR RRKACQACRF TK
NR5A1/SF-1 CPVCGDKV SGYHYGLLTC ESCKGFFKRT VQNNK--HYTCT -ESQSCKIDKT QRKRCPFCRF QK
NR6A1/GCN1 CLICGDRA TGLHYGIISC EGCKGFFKRS ICNKR--VYRCS -RDKNCVMSRK QRNRCQYCRL LK
NR2C1/TR2 CVVCGDKA SGRHYGAVTC EGCKGFFKRS IRKNL--VYSCR -GSKDCIINKH HRNRCQYCRL QR
NR2B1/RXR-alpha CAICGDRS SGKHYGVYSC EGCKGFFKRT VRKDL--TYTCR -DNKDCLIDKR QRNRCQYCRY QK
NR2A1/HNF-4-alpha CAICGDRA TGKHYGASSC DGCKGFFRRS VRKNH--MYSCR -FSRQCVVDKD KRNQCRYCRL KK
NR2F1/COUP1 CVVCGDKS SGKHYGQFTC EGCKSFFKRS VRRNL--TYTCR -ANRNCPIDQH HRNQCQYCRL KK
Trichoplax adhaerens
ERR-like XP_002117375.1 CLVCGDRA SGLHYGVLSC EGCKAFFKRS IQSSV--AYTCP -SGSRCKVDKQ RRKCCQACRL QK
RXR-like XP_002109459.1 CSICGQRS LRRHYGVYSC EGCKGFFKRT VRKNL--TYTCR -DNRNCDIDKK QRNRCQYCRY QK
HNF4-like XP_002115810.1 CAICGDRA TGKHYGASSC DGCKGFFRRS VRKNH--MYSCR -FSRQCVVDKD KRNQCRYCRL KK
COUP-like XP_002109806.1 CLICGDRS NGRHYGVISC EGCKGFFKRS VRRNM--KYACT CSANACKITKA NRNQCQFCRL QK
** *
B
Position 92
Position 94
G92
A92
K94
R94

Figure S3

Figure S3. 3D modeling and sequence conservation of the first zinc finger motif of the RORa DNA-binding domain. (**A**) Sequence comparison of amino acids in the conserved DNA binding domain of human paralogous nuclear receptor proteins and of the four *Trichoplax adhaerens* (primitive metazoan) orthologs. The identifier following "NR" indicates the sub-family to which the nuclear receptors belong. Amino acids that match the consensus sequence are shown in bold and shaded gray. Residue numbering at the top of the alignment corresponds to RORa isoform a. The mutated amino acid cysteine (C) 90, glycine (G) 92, and lysine (K) 94 are indicated on top. Amino acids involved in the P-box are indicated by an asterisk (*). (**B**) Homology model of RORa DNA-binding domain in complex with RORE (ROR DNA response element consisting of the consensus core motif AGGTCA). RORa is depicted in blue as a backbone carbon CA trace and atoms are represented in a standard color scheme. Modeled interaction of RORa isoform a (NP_599023.1) wild type (WT) Gly92 and variant Ala92 (left) or WT Lys94 and variant Arg94 (right) in the recognition a-helix of the RORa DBD with the major groove of DNA. For either mutant, the putative clash between RORa DBD and the DNA are represented by black dotted lines. Clashes between the RORa DBD indicate either distances too short for van der Waals interaction (Ala92-phosphate backbone; left), or for hydrogen bonds (Lys94-guanine-guanine and complementary cytosine; right).

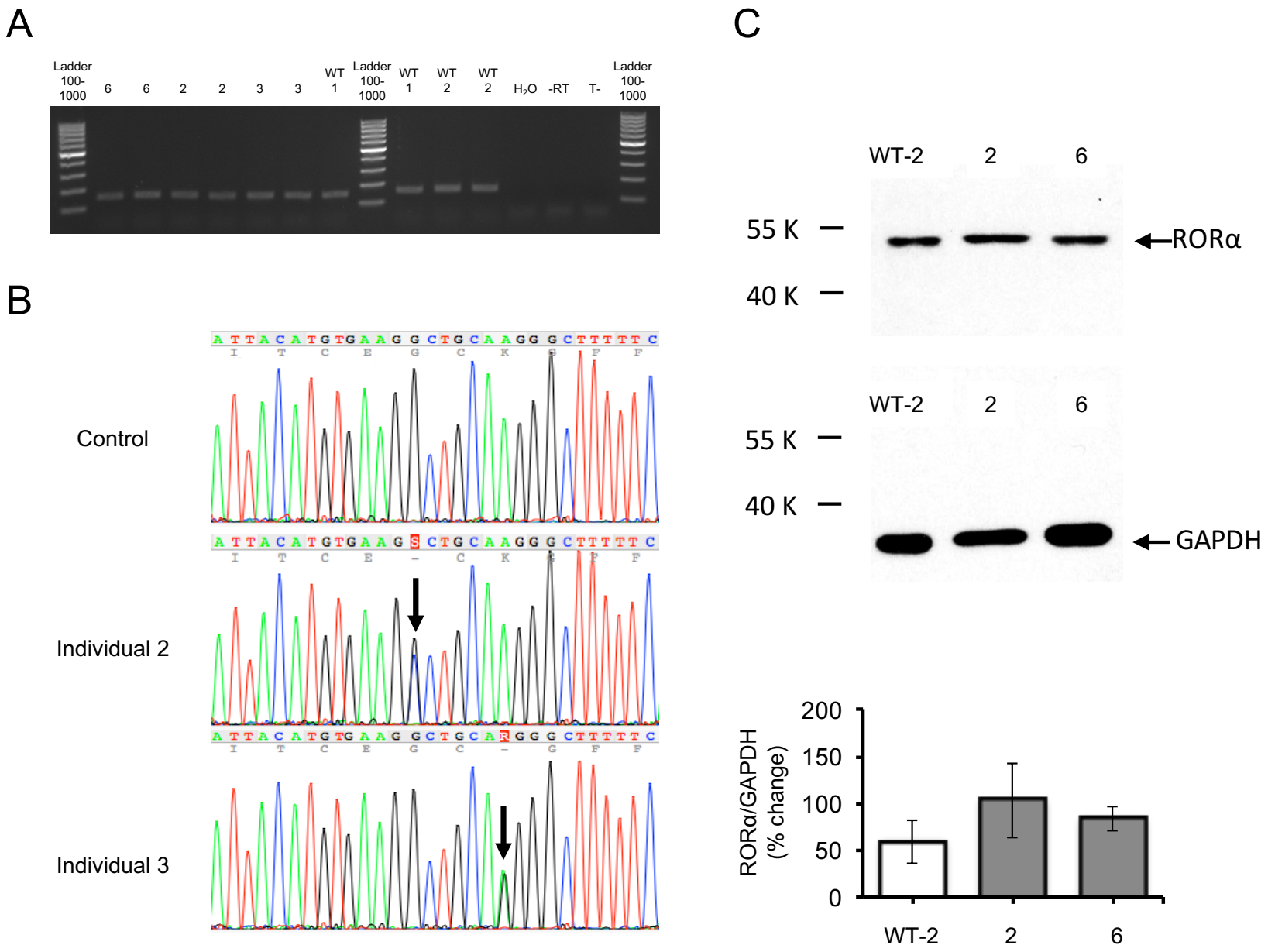
A
Ladder 100-1000
6
6
2
2
3
3
WT 1
Ladder 100-1000
WT 1
WT 2
WT 2
H2O
-RT
T-
Ladder 100-1000
B
Control
Individual 2
Individual 3
C
WT-2
2
6
55 K
40 K
RORα
WT-2
2
6
55 K
40 K
GAPDH
RORα/GAPDH (% change)
200
150
100
50
0
WT-2
2
6

Figure S4

Figure S4. Molecular and biochemical characterization of RORA variants. (**A**) RT-PCR analysis of a 152bp fragment of *RORA* cDNA encompassing the c.281A>G mutation in affected individuals 2, 3 and 6 and control individuals (WT1 and WT2). c.282G is the last nucleotide of exon 3 of *RORA* (NM_134261.2). Neither abnormal sized product nor semi-quantitative variation was observed, suggesting unimpaired splicing. (**B**) Sequencing of the *RORA* RT-PCR products, showing the presence of missense changes c.275G>C (p.Gly92Ala) and c.281A>G (p.Lys94Arg) in individuals 2 and 3, respectively. (**C**) Western blot analysis of protein lysates derived skin fibroblasts established from individual 2 and 6, and control individual WT2. The anti-RORα antibodies were probed against fibroblast cell lysate and revealed a band of the expected size (55 kDa). No smaller product was detected, in particular no truncated fragment was detected for individual 6 bearing a heterozygous frame-shift mutation. The blot was reprobed with anti-GAPDH antibodies. The results show a moderate increase of RORα levels in individual 2 and 6 when compared with wild-type levels as indicated by densitometry analysis. Quantification is based on 3 measurements (individuals 2 and 6) or 4 measurements (WT-2). A representative result of the Western blots is shown. Error bars represent standard error of the mean.

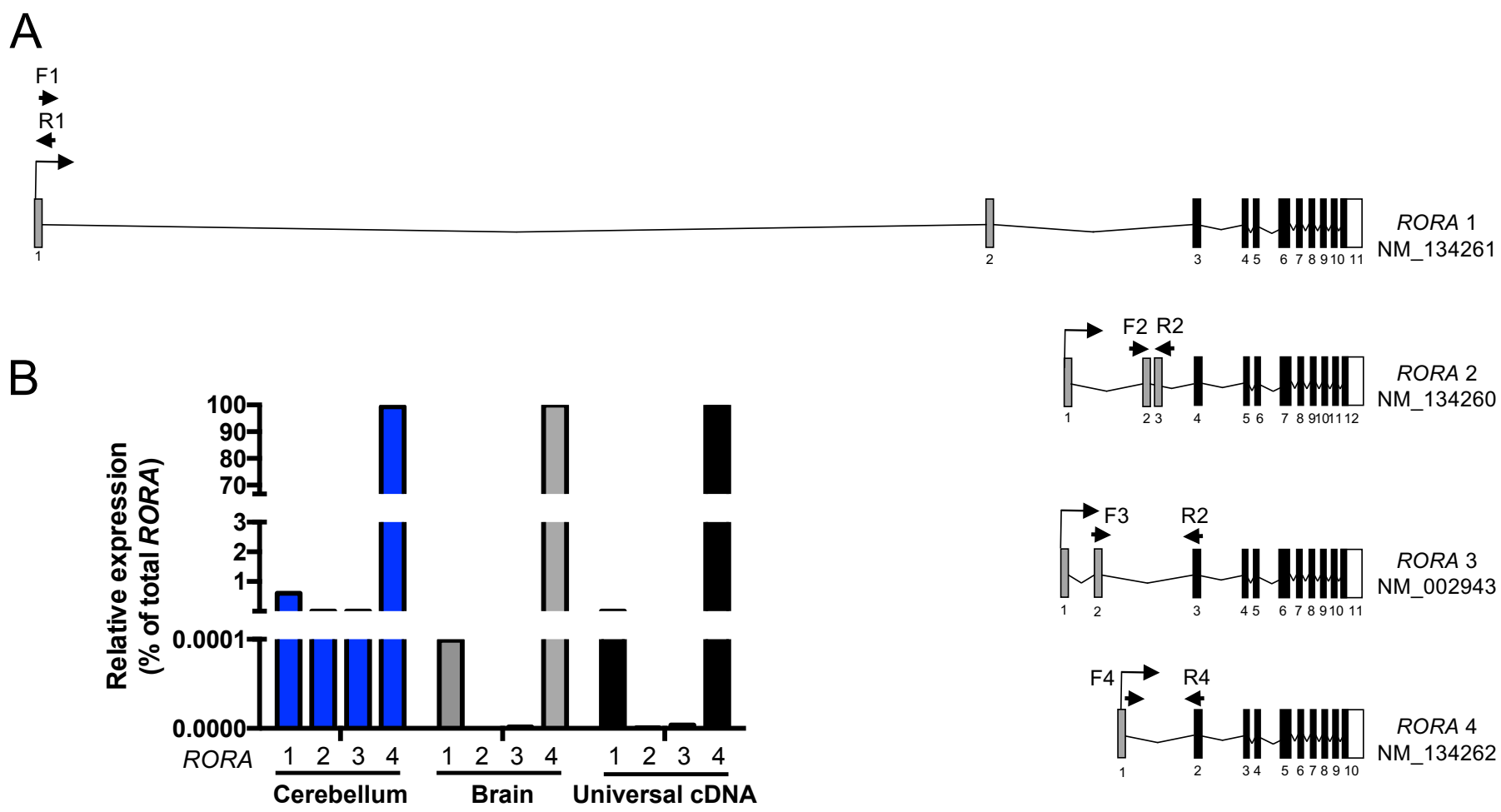
A
F1
R1
1
2
3
4 5
6 7 8 9 10 11
RORA 1
NM_134261
F2 R2
1
2 3
4
5 6
7 8 9 10 11 12
RORA 2
NM_134260
F3
R2
1
2
3
4 5
6 7 8 9 10 11
RORA 3
NM_002943
F4
R4
1
2
3 4
5 6 7 8 9 10
RORA 4
NM_134262
B
Relative expression
(% of total RORA)
100
90
80
70
3
2
1
0.0001
0.0000
RORA
1 2 3 4
1 2 3 4
1 2 3 4
Cerebellum
Brain
Universal cDNA

Figure S5

Figure S5. *RORA* encodes four protein coding splice variants. (**A**) Schematic of the four splice variants expressed from the human *RORA* locus with RefSeq annotations. Gray boxes, coding exons that are unique to each transcript; black boxes, coding exons that are shared among the four transcripts; white boxes, untranslated regions. Arrows indicate position of oligonucleotides used for qRT-PCR experiments. (**B**) *RORA* 4 is the major splice isoform expressed in the central nervous system. qRT-PCR was performed on control adult human cDNA and analyzed by the ΔCt method with normalization to ß-actin mRNA expression. Canonical isoform *RORA* 1 is weakly expressed, as well as *RORA* 2 and *RORA* 3.

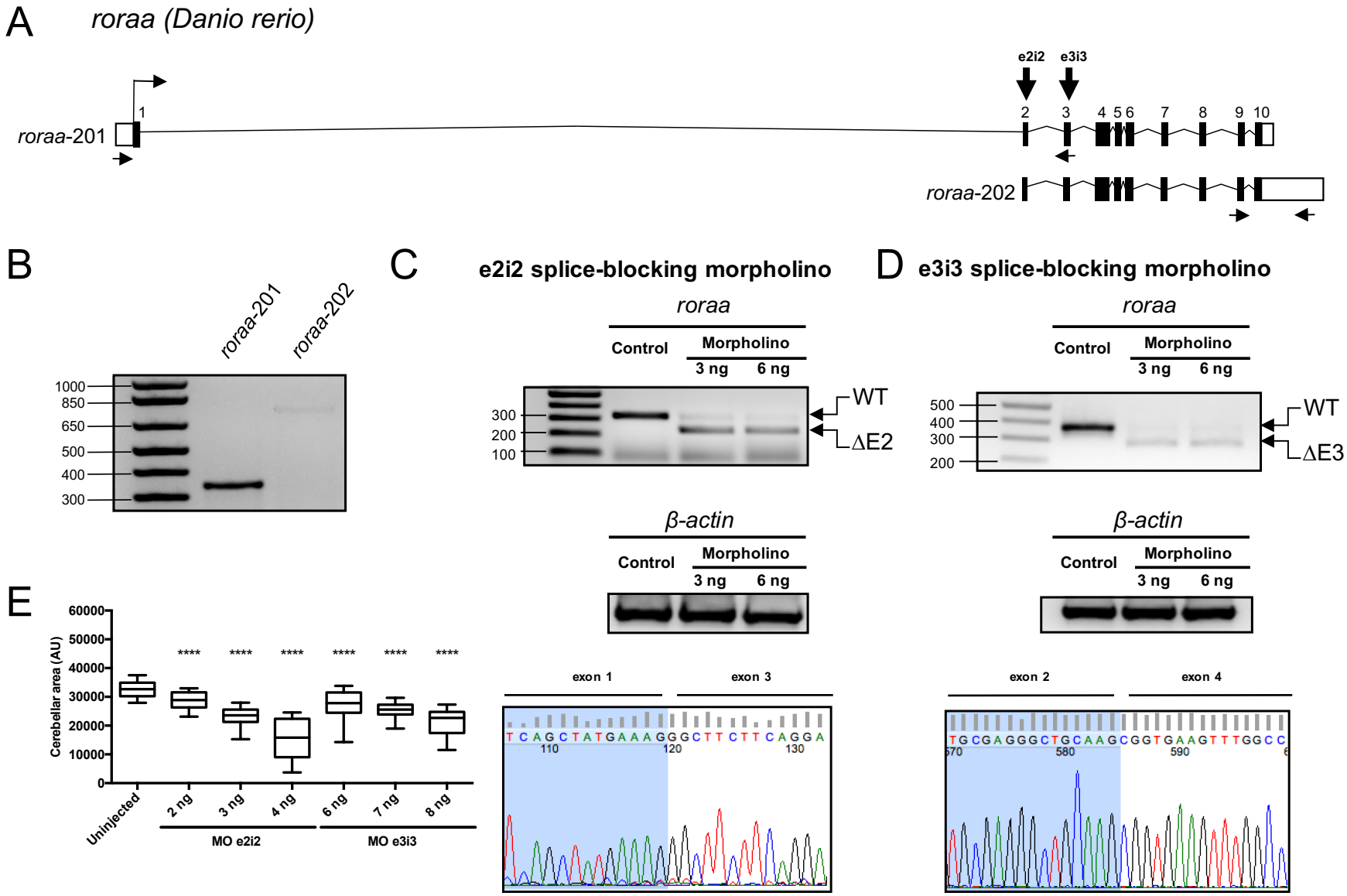
A
roraa (Danio rerio)
roraa-201
roraa-202
e2i2
e3i3
1
2
3
4 5 6
7
8
9 10
B
roraa-201
roraa-202
1000
850
650
500
400
300
C
e2i2 splice-blocking morpholino
roraa
Control
Morpholino
3 ng
6 ng
300
200
100
WT
ΔE2
β-actin
exon 1
exon 3
T C A G C T A T G A A A G G G C T T C T T C A G G A
110
120
130
D
e3i3 splice-blocking morpholino
roraa
Control
Morpholino
3 ng
6 ng
500
400
300
200
WT
ΔE3
β-actin
exon 2
exon 4
T G C G A G G G C T G C A A G C G G T G A A G T T T G G C C
570
580
590
E
Cerebellar area (AU)
60000
50000
40000
30000
20000
10000
0
****
Uninjected
2 ng
3 ng
4 ng
6 ng
7 ng
8 ng
MO e2i2
MO e3i3

Figure S6

Figure S6. *roraa* morpholino targeting efficiency. (**A**) Schematic of two zebrafish *roraa* transcripts, *roraa*-201 and *roraa*-202 (genome assembly Zv10); coding regions, black boxes; untranslated regions, white boxes. Zebrafish *roraa*-201 encodes GenBank ID: NP_001103637 (95% similar; 91% identical to human RORA 4). Vertical arrows indicate splice-blocking (sb) morpholino (MO) target sites on the donor sites of exons 2 and 3, respectively; horizontal arrows indicate RT-PCR primers used to generate amplicons in panel **B**. (**B**) *roraa*-201 and *rora*-202 are detectable in zebrafish during larval development (3 days post-fertilization, dpf). Agarose gel image showing RT-PCR results obtained by using isoform-specific primers (shown in panel **A**). (**C**) Agarose gel images (top), and chromatograms of TOPO-cloned PCR product (bottom) demonstrate that the e2i2 sb MO induces exclusion of exon 2 (DE2) leading to a frameshift and introduction of a premature stop codon (p.Ile62*); WT, wild-type transcript. (**D**) Agarose gel images (top), and chromatogram of TOPO-cloned PCR product (bottom) shows that the e3i3 sb MO leads to skipping of exon 3 (DE3) leading to a frameshift and premature stop codon (p.Val88*). (**E**) *roraa* e2i2 or e3i3 sb MOs lead to dose-dependent reduction of cerebellar size in 3 dpf larval batches immunostained with anti-acetylated tubulin antibody. Stars indicate *P* value compared to WT; ****, $p<0.0001$. Error bars in (**E**) re-present 5th and 95th Percentile.

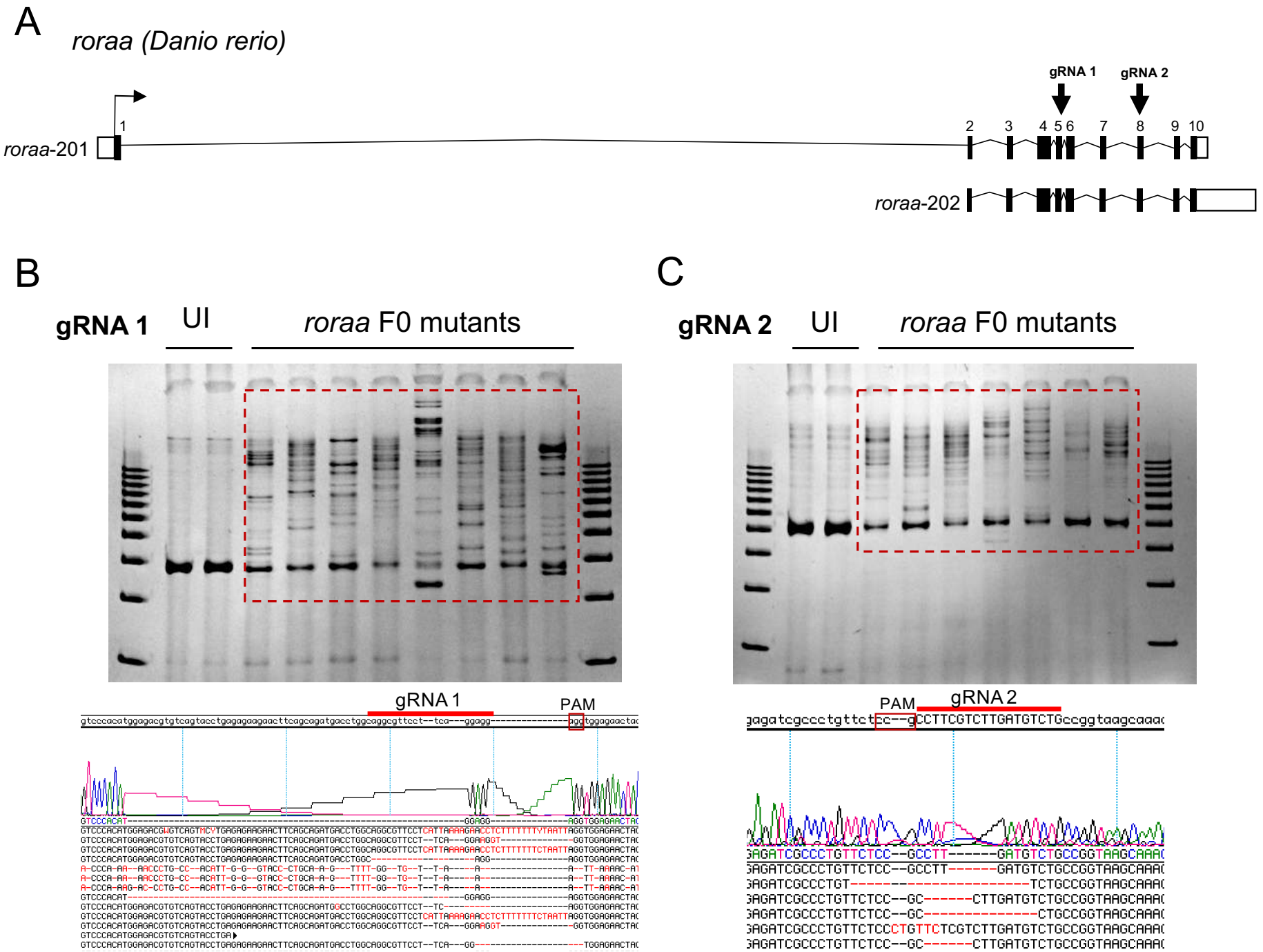
A
roraa (Danio rerio)
gRNA 1
gRNA 2
roraa-201
1
2 3 4 5 6 7 8 9 10
roraa-202
B
gRNA 1
UI
roraa F0 mutants
gRNA 1
PAM
C
gRNA 2
UI
roraa F0 mutants
PAM
gRNA 2

Figure S7

Figure S7. *roraa* CRISPR/Cas9 genome editing efficiency. (**A**) Schematic of two zebrafish *roraa* transcripts, *roraa*-201 and *roraa*-202 (genome assembly Zv10); coding regions, black boxes; untranslated regions, white boxes. guide (g)RNA target sites are by vertical arrows on exons 5 and 8. (**B** and **C**) Top, CRISPR/Cas9 targeting of *roraa* F0 mutant embryos leads to small insertion and deletion events detectable by heteroduplex formation; PCR products flanking target sites were amplified, denatured, slowly reannealed and migrated on a polyacrylamide gel (n=2 uninjected [UI] controls and 8 or 7 F0 mutants for gRNA 1 and gRNA 2, respectively). Heteroduplexes are indicated by red boxes. Bottom, representative chromatograms indicating insertion and deletion events at the gRNA target. gRNA sequence and protospacer adjacent motifs (PAM) are shown. We sequenced 3 F0 mutants/gRNA and 24 colonies per embryo to confirm >90% mosaicism for both gRNA 1 and gRNA 2.

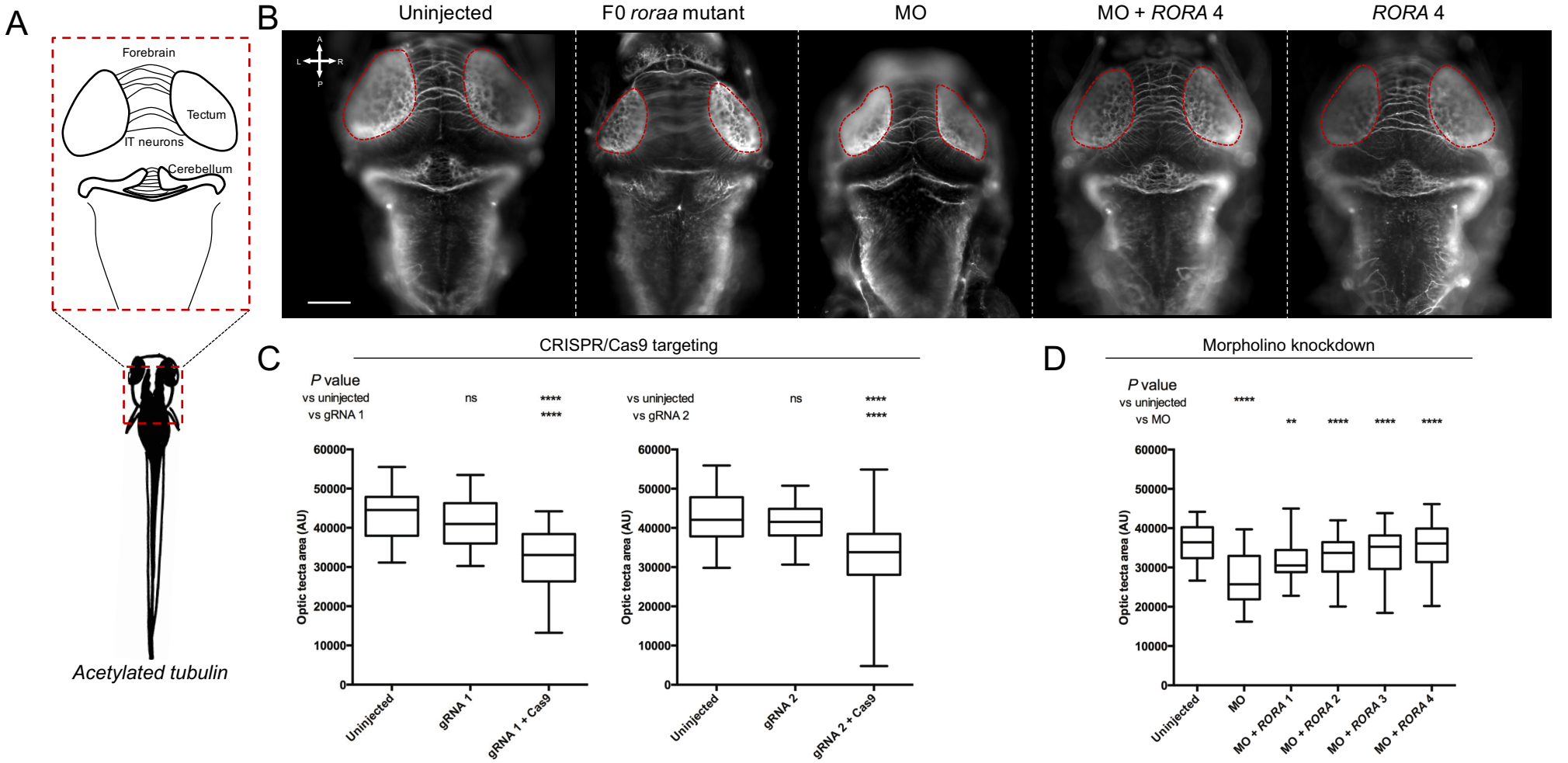
A
Forebrain
Tectum
IT neurons
Cerebellum
Acetylated tubulin
B
Uninjected
F0 roraa mutant
MO
MO + RORA 4
RORA 4
C
CRISPR/Cas9 targeting
P value
vs uninjected
vs gRNA 1
ns
****
****
vs uninjected
vs gRNA 2
ns
****
****
Optic tecta area (AU)
60000
50000
40000
30000
20000
10000
0
Uninjected
gRNA 1
gRNA 1 + Cas9
Uninjected
gRNA 2
gRNA 2 + Cas9
D
Morpholino knockdown
P value
vs uninjected
vs MO
****
**
****
****
****
Optic tecta area (AU)
Uninjected
MO
MO + RORA 1
MO + RORA 2
MO + RORA 3
MO + RORA 4

Figure S8

Figure S8. Disruption of *roraa* in zebrafish larvae results in a reduction of optic tecta size. (**A**) Schematic of neuroanatomical structures painted with anti-acetylated tubulin antibody at 3 days post fertilization (dpf); IT, intertectal. (**B**) Representative dorsal images of acetylated tubulin immunostained larvae show that *roraa* ablation causes neuroanatomical defects in CRISPR/Cas9 F0 mutants and morphants. Optic tecta size was measured as indicated by the dashed red outline on inset panels. Scale bar: 100 μm. (**C**) Quantification of tecta area in larval batches is shown for two guide (g)RNAs targeting either *roraa* exon 5 (gRNA 1) or exon 8 (gRNA 2) (**D**) *roraa* morphants (injected with 3 ng morpholino; MO) display a neuroanatomical phenotype that can be rescued by four different wild type *RORA* mRNA transcripts: co-injection of *roraa* e2i2 splice-blocking MO with *RORA* splice variants (*RORA* 1: NM_134261, *RORA* 2: NM_134260, *RORA* 3: NM_002943 and *RORA* 4: NM_134262). AU, arbitrary units. Stars indicate *P* value compared to uninjected controls (CRISPR/Cas9 and MO) or to morphants (MO + RORA). ****, $p<0.0001$; **, $p<0.01$; ns, not significant. Error bars in (**C**) and (**D**) represent 5th and 95th Percentile.

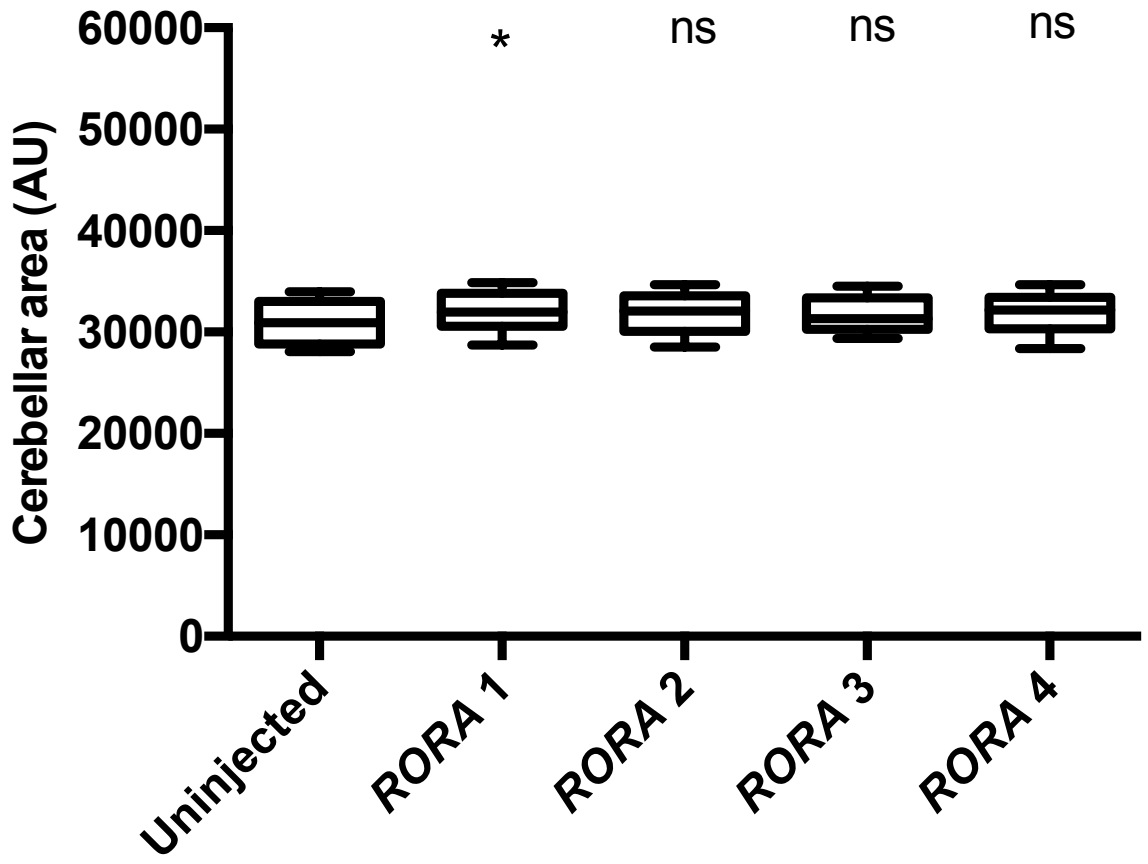
60000
50000
40000
30000
20000
10000
0
Cerebellar area (AU)
*
ns
ns
ns
Uninjected
RORA 1
RORA 2
RORA 3
RORA 4

Figure S9

Figure S9. Ectopic expression of human WT *RORA* in zebrafish larvae. *In vivo* ectopic expression of *RORA* splice variants does not induce cerebellar abnormalities. Zebrafish embryos were injected with 200 pg of wild-type *RORA* mRNA corresponding to each of the four protein coding isoforms, stained with acetylated tubulin antibody, imaged and measured (see Figure 3). AU, arbitrary units. *P* values are not significant (ns) except for *RORA* 1: $P=0.03$ (bilateral t-test). Error bars represent 5th and 95th Percentile.

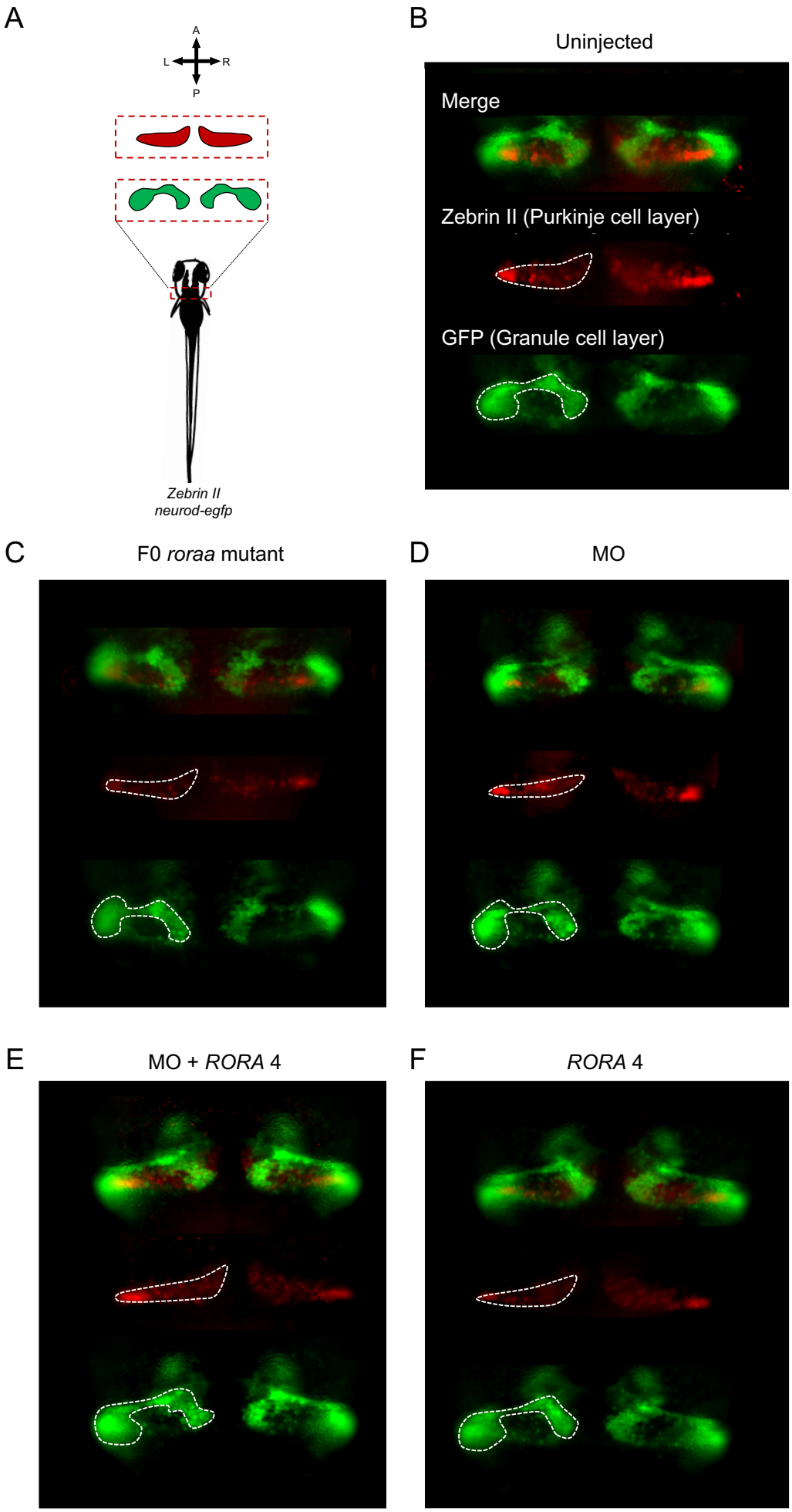
A
A
L
R
P
Zebrin II
neurod-egfp
B
Uninjected
Merge
Zebrin II (Purkinje cell layer)
GFP (Granule cell layer)
C
F0 roraa mutant
D
MO
E
MO + RORA 4
F
RORA 4

Figure S10

Figure S10. Disruption of *roraa* in zebrafish larvae results in cerebellar hypoplasia driven by Purkinje and granule cell loss. (**A**) Schematic of cerebellar cell types assessed in 3 dpf larvae using either a *neurod:egfp* transgene (green) or anti-zebrin II immunostaining (red). Orientation is indicated with A, anterior; P, posterior; L, left; R, right. (**B-F**) Representative dorsal images show that reduction of Purkinje and granule cells contributes to cerebellar defects induced by *roraa* targeting. Transgenic *neurod:egfp* larvae were fixed, immunostained with anti-zebrin II antibody (red), and the area comprised of each cell type was measured (as indicated in the schematic; see Figure 3E-H). Dashed white lines indicate measured area in (**B**) uninjected larvae; (**C**) larvae injected with CRISPR/Cas9 cocktail; (**D**) e2i2 splice-blocking morpholino (MO); (**E**) MO co-injected with wild-type *RORA* 4 mRNA; or (**F**) wild-type *RORA* mRNA alone.